

Unitary Ca^{2+} current through recombinant type 3 InsP_3 receptor channels under physiological ionic conditions

Horia Vais,¹ J. Kevin Foskett,^{1,2} and Don-On Daniel Mak¹

¹Department of Physiology and ²Department of Cell and Developmental Biology, University of Pennsylvania School of Medicine, Philadelphia, PA 19104

The ubiquitous inositol 1,4,5-trisphosphate (InsP_3) receptor (InsP_3R) channel, localized primarily in the endoplasmic reticulum (ER) membrane, releases Ca^{2+} into the cytoplasm upon binding InsP_3 , generating and modulating intracellular Ca^{2+} signals that regulate numerous physiological processes. Together with the number of channels activated and the open probability of the active channels, the size of the unitary Ca^{2+} current (i_{Ca}) passing through an open InsP_3R channel determines the amount of Ca^{2+} released from the ER store, and thus the amplitude and the spatial and temporal nature of Ca^{2+} signals generated in response to extracellular stimuli. Despite its significance, i_{Ca} for InsP_3R channels in physiological ionic conditions has not been directly measured. Here, we report the first measurement of i_{Ca} through an InsP_3R channel in its native membrane environment under physiological ionic conditions. Nuclear patch clamp electrophysiology with rapid perfusion solution exchanges was used to study the conductance properties of recombinant homotetrameric rat type 3 InsP_3R channels. Within physiological ranges of free Ca^{2+} concentrations in the ER lumen ($[\text{Ca}^{2+}]_{\text{ER}}$), free cytoplasmic Ca^{2+} ($[\text{Ca}^{2+}]_i$), and symmetric free $[\text{Mg}^{2+}]$ ($[\text{Mg}^{2+}]_f$), the $i_{\text{Ca}}-[\text{Ca}^{2+}]_{\text{ER}}$ relation was linear, with no detectable dependence on $[\text{Mg}^{2+}]_f$. i_{Ca} was $0.15 \pm 0.01 \text{ pA}$ for a filled ER store with $500 \text{ }\mu\text{M} [\text{Ca}^{2+}]_{\text{ER}}$. The $i_{\text{Ca}}-[\text{Ca}^{2+}]_{\text{ER}}$ relation suggests that Ca^{2+} released by an InsP_3R channel raises $[\text{Ca}^{2+}]_i$ near the open channel to $\sim 13\text{--}70 \text{ }\mu\text{M}$, depending on $[\text{Ca}^{2+}]_{\text{ER}}$. These measurements have implications for the activities of nearby InsP_3 -liganded InsP_3R channels, and they confirm that Ca^{2+} released by an open InsP_3R channel is sufficient to activate neighboring channels at appropriate distances away, promoting Ca^{2+} -induced Ca^{2+} release.

INTRODUCTION

Modulating cytoplasmic free Ca^{2+} concentration ($[\text{Ca}^{2+}]_i$) is a ubiquitous intracellular signaling pathway that regulates numerous cellular physiological processes, including apoptosis, gene expression, bioenergetics, secretion, immune responses, fertilization, muscle contraction, synaptic transmission, and learning and memory (Clapham, 1995; Berridge et al., 2000; Bootman et al., 2001; Braet et al., 2004; Randriamampita and Trautmann, 2004; Cárdenas et al., 2010b). The inositol 1,4,5-trisphosphate (InsP_3) receptor (InsP_3R), a transmembrane protein localized mainly at the ER in all animal cell types, plays a central role in this $[\text{Ca}^{2+}]_i$ signaling pathway (Taylor and Richardson, 1991; Bezprozvanny and Ehrlich, 1995; Furuichi and Mikoshiba, 1995; Patterson et al., 2004; Foskett et al., 2007; Joseph and Hajnóczky, 2007). In response to extracellular stimuli, phosphatidylinositol 4,5-bisphosphate in the plasma membrane is hydrolyzed to generate InsP_3 (Berridge, 1993). InsP_3 rapidly diffuses through the cytoplasm to bind to the InsP_3R and activates it as an intracellular Ca^{2+} channel to release Ca^{2+} stored inside the lumen of the ER into the cyto-

plasm, generating diverse local and global $[\text{Ca}^{2+}]_i$ signals (Berridge, 1997).

The InsP_3R -mediated Ca^{2+} flux from the ER store in response to various extracellular stimuli is $\propto N_{\text{A}} i_{\text{Ca}} P_o$, where N_{A} is the number of InsP_3R channels activated, i_{Ca} is the unitary calcium ion current passing through an individual open InsP_3R channel, and P_o is the open probability of the active InsP_3R channels. The amount of Ca^{2+} released, and therefore the amplitude and spatial and temporal nature of the $[\text{Ca}^{2+}]_i$ signals generated, is directly dependent on i_{Ca} (Berridge, 1997; Bootman et al., 1997). Furthermore, the P_o of InsP_3R channels is regulated by $[\text{Ca}^{2+}]_i$ with a biphasic dependence: at low concentrations, Ca^{2+} activates the channel and increases its P_o , whereas at higher concentrations, Ca^{2+} inhibits the channel (Foskett et al., 2007). Consequently, i_{Ca} also affects indirectly the amount of Ca^{2+} released by regulating the P_o of the activated channel itself, as well as that of nearby surrounding channels. Therefore, the measurement of i_{Ca} in ionic conditions similar to those that exist physiologically in cells is critical for the

Correspondence to: Don-On Daniel Mak: dmak@mail.med.upenn.edu

Abbreviations used in this paper: i_{Ca} , unitary Ca^{2+} current; InsP_3 , inositol 1,4,5-trisphosphate; InsP_3R , InsP_3 receptor.

understanding of the mechanisms regulating this important signaling pathway.

Although InsP_3R channel activity level (P_o) and the number of channels activated (N_A) under various physiological conditions have been studied previously by electrophysiological methods, especially single-channel nuclear patch clamp experiments in various configurations (Foskett et al., 2007), the unitary Ca^{2+} current (i_{Ca}) passing through an open InsP_3R channel has not been characterized, primarily as a consequence of technical difficulties. Here, we measured the i_{Ca} of recombinant homotetrameric rat type 3 InsP_3R channels under physiological ionic conditions and studied its single-channel conductance properties.

MATERIALS AND METHODS

Nucleus isolation and nuclear patch clamp electrophysiology

The generation and maintenance of DT40-KO-r- InsP_3R -3 cells (mutant cells derived from chicken B cells with the endogenous genes for all three InsP_3R isoforms knocked out and then stably transfected to express recombinant rat type 3 InsP_3R) were described in Mak et al. (2005). Nuclear patch clamp experiments were performed using nuclei isolated from DT40-KO-r- InsP_3R -3 cells as described previously (Mak et al., 2005). Excised nuclear membrane patches in the luminal side-out (lum-out) or cytoplasmic side-out (cyto-out) configuration were obtained from isolated nuclei (Mak et al., 2007) using protocols analogous to those used to obtain inside-out or outside-out excised patches in plasma membrane patch clamp experiments. The solution around the excised nuclear membrane patch was rapidly switched multiple times using a solution-switching setup described in Mak et al. (2007).

InsP_3R channel current traces were acquired at room temperature as described previously (Mak et al., 1998), digitized at 5 kHz, and anti-aliasing filtered at 1 kHz. Data analysis and the fitting of channel current–voltage curves were performed using Igor-Pro software. All electrical potentials were measured relative to the bath electrode.

Experimental solution composition

In cyto-out experiments, pipette solutions contained 140 mM KCl, 10 mM HEPES, pH to 7.3 with KOH, 0.5 mM Na_2ATP , and 10 μM InsP_3 , with free $[\text{Ca}^{2+}]_f$ ($[\text{Ca}^{2+}]_f$) buffered to 3 μM by 0.5 mM 5,5'-dibromo 1,2-bis(o-aminophenoxy) ethane-*N,N,N',N'*-tetraacetic acid (dibromo BAPTA) and 0.2 mM CaCl_2 . Perfusion solutions on the cytoplasmic side of the channel contained 10 mM HEPES, pH to 7.3 with KOH, 0.5 mM Na_2ATP , and either 140 mM KCl with no InsP_3 or 70 mM KCl with 10 μM InsP_3 , with $[\text{Ca}^{2+}]_f$ buffered to 3 μM by 0.5 mM (2-hydroxyethyl) ethylenediaminetetraacetate and 0.22 mM CaCl_2 (Mak et al., 2005). InsP_3 and Na_2ATP were included in the pipette solution to confirm that the cyto-out configuration was properly achieved. Because of the presence of InsP_3 and ATP in the pipette solution, observation of InsP_3R channel activity before solution switching would be evidence that the lum-out configuration was erroneously obtained.

The same pipette solution was used in lum-out experiments to determine ion permeability ratios of the InsP_3R channel. The perfusion solution used to determine $P_{\text{K}}:P_{\text{Cl}}$ contained 30 mM KCl, 110 mM NMDG chloride, and 10 mM HEPES, pH to 7.3 with NMDG, with $[\text{Ca}^{2+}]_f$ buffered to 300 nM by 0.5 mM 1,2-bis(o-aminophenoxy) ethane-*N,N,N',N'*-tetraacetic acid (BAPTA) and 0.2 mM CaCl_2 . The perfusion solution used to determine $P_{\text{K}}:P_{\text{Na}}$ contained 140 mM NaCl and 10 mM HEPES, pH to 7.3 with NaOH.

The perfusion solution used to determine $P_{\text{X}}:P_{\text{K}}$ ($\text{X} = \text{Mg}^{2+}$, Ca^{2+} , Sr^{2+} , or Ba^{2+}) contained 140 mM KCl, 10 mM HEPES, pH to 7.3 with KOH, and 10 mM XCl_2 . The perfusion solutions contained no Na_2ATP or Ca^{2+} chelator. No CaCl_2 was added to the perfusion solutions used to determine permeability ratios of Mg^{2+} , Sr^{2+} , and Ba^{2+} versus K^+ , so free Ca^{2+} in those solutions were from contaminants in the water and salts used to make the solutions. Based on the purity assays of the salts (Sigma-Aldrich) and induction-coupled plasma mass spectrometry assay (Mayo Medical Laboratory) of deionized water samples, $[\text{Ca}^{2+}]_f$ in those solutions were $\sim 5\text{--}8 \mu\text{M}$.

In lum-out experiments to determine the i_{Ca} through the InsP_3R -3 channel, all solutions contained 10 mM HEPES, pH to 7.3 with KOH. Unless stated otherwise, all solutions used in the same experiment contained the same concentrations of MgCl_2 (0, 0.5, or 1 mM), KCl (140 or 40 mM), and potassium methanesulfonate (KCH_3SO_3 ; 0 or 100 mM). Pipette solutions also contained 0.5 mM Na_2ATP and 2 or 10 μM InsP_3 to activate the channel to P_o of ~ 0.5 (Mak et al., 2001a,b; Vais et al., 2010), with $[\text{Ca}^{2+}]_f$ buffered to either 70 nM by 0.5 mM BAPTA and 0.06 mM CaCl_2 , or to 3 μM by 0.5 mM dibromo BAPTA and 0.2 mM CaCl_2 . The same solution (without Na_2ATP or InsP_3) was used as perfusion solution for symmetric ionic conditions. Although $[\text{Na}^+]$ was not symmetric because of the presence of 0.5 mM Na_2ATP only in the pipette solutions, the extra Na^+ is $<1\%$ of the amount of monovalent cations, and its contribution to channel current is negligible. Perfusion solutions used for asymmetric ionic conditions contained 0.3, 1, or 2 mM CaCl_2 , with no Ca^{2+} chelator, Na_2ATP , or InsP_3 .

$[\text{Ca}^{2+}]_f$ of $<100 \mu\text{M}$ (buffered by various Ca^{2+} chelators) was confirmed by fluorimetry. $[\text{Ca}^{2+}]_f$ in solutions without Ca^{2+} chelators was calculated using activity coefficients (see next section).

Evaluating ion permeability ratios

According to the general Goldman-Hodgkin-Katz current equation (Lewis, 1979), the permeability ratio $P_{\text{Y}}/P_{\text{K}}$ for Y, one of the charge-carrying permeant ion species, can be evaluated from the reversal potential (V_{rev}) of the channel as:

$$P_{\text{Y}}:P_{\text{K}} = -(z_{\text{Y}})^{-2} \left\{ \frac{[\text{Y}]_i - [\text{Y}]_o \exp(-z_{\text{Y}}FV_{\text{rev}}/RT)}{1 - \exp(-z_{\text{Y}}FV_{\text{rev}}/RT)} \right\}^{-1} \\ \sum_{\text{X} \neq \text{Y}} \left\{ \left(\frac{P_{\text{X}}}{P_{\text{K}}} \right) (z_{\text{X}})^2 \frac{[\text{X}]_i - [\text{X}]_o \exp(-z_{\text{X}}FV_{\text{rev}}/RT)}{1 - \exp(-z_{\text{X}}FV_{\text{rev}}/RT)} \right\}, \quad (1)$$

where X represents other permeant ion species present; P_{X} is the permeability of X through the channel; z_{X} and z_{Y} are the valence of X and Y, respectively; $[\text{X}]_i$, $[\text{X}]_o$, $[\text{Y}]_i$, and $[\text{Y}]_o$ are the activities of X and Y in the pipette and bath solutions, respectively; F and R are the Faraday and gas constants, respectively; and T is the absolute temperature, provided that all of the $P_{\text{X}}/P_{\text{K}}$ values are known. The activities of all ion species were calculated from activity coefficients, except for $[\text{Ca}^{2+}] < 100 \mu\text{M}$, which was determined by fluorimetry.

The activity coefficients of KCl and NaCl were calculated using the Debye-Hückel equation based on data reported by Hamer and Wu (1972). The activity coefficients of CaCl_2 in a 140-mM KCl solution (0.546–0.534 for 0.3–10 mM CaCl_2) were derived by interpolation using data reported by Butler (1968), assuming that CaCl_2 activity coefficients are similar in 140-mM KCl and NaCl solutions. The activity coefficients of CaCl_2 were used for other alkaline earth metal halides (MgCl_2 , BaCl_2 , and SrCl_2) in solutions with the same concentrations because activity coefficients of the alkaline earth metal halides differ by $<5\%$ in concentrations when activity coefficients are ≈ 0.54 (Goldberg and Nuttall, 1978).

RESULTS

Conductance properties of homotetrameric recombinant rat $\text{InsP}_3\text{R-3}$ channels

Although it has been a well-established approach to study the single-channel properties of the InsP_3R channel in its native membrane environment by performing patch clamp electrophysiology on isolated nuclei (Foskett et al., 2007), the molecular composition of the channels observed in many of those studies could not be definitively ascertained. This is because the channels studied were either the endogenous channels (Mak and Foskett, 1994, 1997; Marchenko et al., 2005; Ionescu et al., 2006) with the possibility of different channel isoforms expressed and with possible alternative splicing (Foskett et al., 2007), or recombinant channels expressed in cells with a non-zero level of endogenous InsP_3R expression (Mak et al., 2000; Boehning et al., 2001a), so that heterooligomeric channels of recombinant and endogenous InsP_3Rs could have been formed (Joseph et al., 1995; Mak et al., 2000).

To avoid possible variability that such heterogeneity might introduce, we ensured that only homotetrameric InsP_3R channels with known identical amino acid sequences were studied by using a stably transfected cell line (DT40-KO-r- $\text{InsP}_3\text{R-3}$) derived from mutant DT40- $\text{InsP}_3\text{R-KO}$ cells (Sugawara et al., 1997) that have all endogenous genes for the three InsP_3R isoforms knocked out, with only recombinant rat type 3 InsP_3R ($\text{InsP}_3\text{R-3}$) expressed (Mak et al., 2005; Li et al., 2007). During our

extensive experience working with this cell line (Mak et al., 2005; Foskett and Mak, 2010), and in hundreds of nuclear membrane patches (in both cyto-out and lum-out configurations), only one kind of channel with a conductance >100 pS in symmetric 140 mM KCl was detected. The identity of these channels as recombinant rat $\text{InsP}_3\text{R-3}$ channels was confirmed by their sensitivity to activation by cytoplasmic InsP_3 (Fig. 1 A).

Averaged over reasonable intervals (>1 s), the rat $\text{InsP}_3\text{R-3}$ channel dwells in a main open conductance state $>95\%$ of the time it is open, whereas it occasionally exhibits brief substates of lower conductances (Fig. 1, A and B). The substates are not a result of non- InsP_3R channels because in current records showing only one active InsP_3R channel gating, the channel current level dropped to substate levels from the main open state directly without channel closing (Fig. 1 B, arrowheads). Substates have also been observed for other InsP_3R channels (endogenous or recombinant) in other cell systems (Watras et al., 1991; Mak and Foskett, 1997; Mak et al., 2000; Boehning et al., 2001a; Ionescu et al., 2006). To determine the conductance of the main open state of the channel in symmetric 140-mM KCl solutions ($[\text{K}^+]_f = [\text{Cl}^-]_f \approx 104$ mM) in the absence of Mg^{2+} , currents through excised lum-out membrane patches (I) were recorded as the applied potential (V_{app}) was ramped (Fig. 1 C). Slope conductance of the channel (g_{ch}), evaluated as the difference between the slopes of the fits to open- and closed-channel current (I_{open} and I_{closed} ,

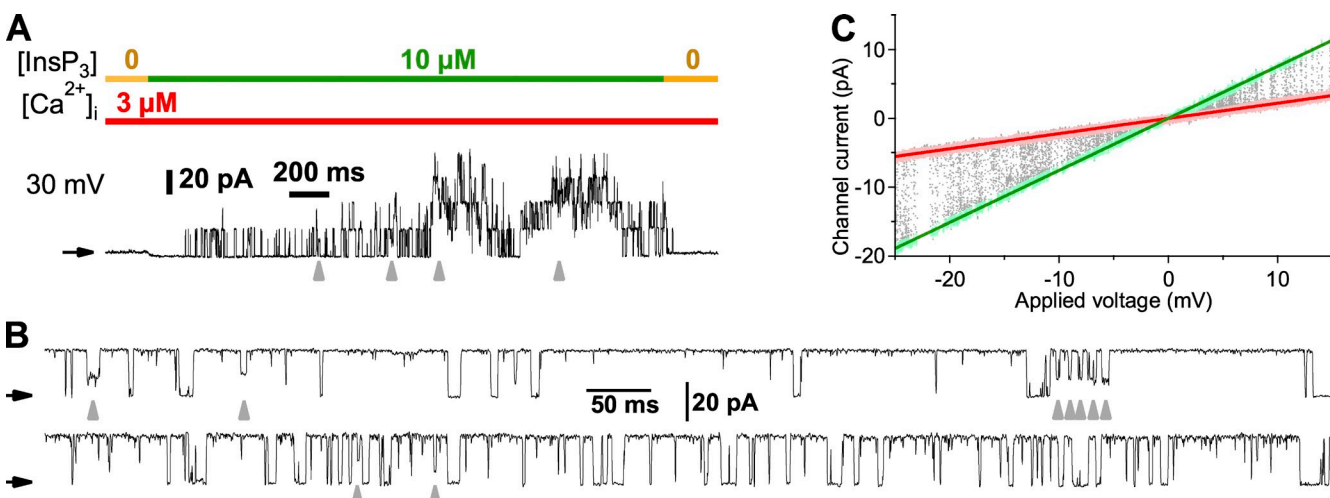


Figure 1. Current records of homotetrameric recombinant type 3 InsP_3R channels in membrane patches excised from nuclei isolated from DT40-KO-r- $\text{InsP}_3\text{R-3}$ cells. (A) Activation by InsP_3 of channels in a cyto-out nuclear membrane patch. Concentrations of InsP_3 and free Ca^{2+} in the perfusion solution on the cytoplasmic side of the channel are indicated by color bars at top. $V_{\text{app}} = 30$ mV. Channels opened only in the presence of cytoplasmic InsP_3 . Gray arrowheads indicate some of the occasions when one of the active channels entered a conductance substate. In this and subsequent current traces, black arrows indicate the membrane current levels when all InsP_3R channels in the membrane patch were closed. (B) Single $\text{InsP}_3\text{R-3}$ channel current records observed in different lum-out nuclear patches in symmetric 140 mM KCl and 3 μM $[\text{Ca}^{2+}]_i$. Pipette solution contained 10 μM InsP_3 . $V_{\text{app}} = 40$ mV. Gray arrowheads indicate when the channels entered different conductance substates with different conductance values. (C) Representative $I-V_{\text{app}}$ plot for a single $\text{InsP}_3\text{R-3}$ channel in the same experimental conditions as in B. V_{app} was ramped from -25 to 15 mV in 1 s. 20 ramps were analyzed. Data points selected for I_{open} and I_{closed} are plotted in green and pink, respectively. Green and red lines represent linear fits to I_{open} and I_{closed} data points, respectively.

respectively) data, was 545 ± 7 pS ($n = 16$). This and all subsequent open-channel current measurements were not affected by the presence of substates because atypical current data arising from them were excluded when data points were selected for I - V_{app} fits.

To properly design an experimental approach to measure the i_{Ca} passing through a single open $InsP_3R$ -3 channel under physiological ionic conditions, it was useful to obtain a maximum estimate of the size of the current using the Goldman-Hodgkin-Katz current equation (Hille, 2001). To obtain such an estimate requires knowledge of the permeability values of all permeant ionic species present. To evaluate the permeabilities of various ions through the $InsP_3R$ -3 channel, I - V_{app} data were recorded as V_{app} was ramped during a series of lum-out patch clamp experiments in which the excised membrane patches were exposed to asymmetric ionic conditions (Fig. 2). After correcting for liquid junction potentials (Neher, 1995), the reversal potential (V_{rev}) of the channel was determined as the V_{app} at the intersection of the I_{open} - V_{app} and I_{closed} - V_{app} fits. Permeability ratios for various ions were calculated from V_{rev} using the general Goldman-Hodgkin-Katz current equation (Eq. 1). The permeability ratio for K^+ versus Cl^- ($P_K:P_{Cl}$) was derived using asymmetric ionic solutions containing only two permeant ionic species: K^+ and Cl^- (Fig. 2 A). That value was then used to calculate the permeability ratios of other cations (Mg^{2+} , Ca^{2+} , as well as Ba^{2+} , Sr^{2+} , and Na^+) versus K^+ from V_{rev} measured in asymmetric ionic solutions containing three permeant ionic species (Fig. 2, B-F), assuming that $P_K:P_{Cl}$ is the same in all ionic conditions used. These measurements indicated that $P_{Ca}:P_{Sr}:P_{Ba}:P_{Mg}:P_{Na}:P_K:P_{Cl} = (15.2 \pm 0.6):(13.2 \pm 0.7):(11.8 \pm 0.5):(10.2 \pm 0.3):(1.24 \pm 0.003):1:(0.27 \pm 0.01)$ ($n = 3$ for each ratio). This same $InsP_3R$ permeability ratio sequence was also observed in other nuclear patch clamp experiments (Mak and Foskett, 1998; Mak et al., 2000; Boehning et al., 2001a; Ionescu et al., 2006).

i_{Ca} through $InsP_3R$ -3 under physiological conditions

Although the $InsP_3R$ channel has a large g_{ch} in solutions with physiological KCl concentrations, the current measured under those conditions is mostly carried by K^+ ions driven through the channel by V_{app} . Because of the absence of a significant voltage across the ER membrane (Beeler et al., 1981; Marhl et al., 1997), Ca^{2+} ions are driven through open $InsP_3R$ channels under physiological conditions by the difference between $[Ca^{2+}]_f$ in the ER lumen ($[Ca^{2+}]_{ER}$) and that in the cytoplasm ($[Ca^{2+}]_i$). $[Ca^{2+}]_{ER}$ observed in various cell types is approximately hundreds of micromolars (Bygrave and Benedetti, 1996; Yu and Hinkle, 2000; Palmer et al., 2004), so there are significantly fewer Ca^{2+} ions than K^+ ions to carry the current. A simple calculation based on the Goldman-Hodgkin-Katz current equation suggests that, in the absence of transmembrane voltage, with $[Ca^{2+}]_{ER} = 1$ mM

and $[Ca^{2+}]_i = 70$ nM, i_{Ca} is ~ 3 pA for a channel with $g_{ch} = 545$ pS in 140 mM KCl and $P_{Ca}:P_K:P_{Cl} = 15:1:0.27$. However, the actual i_{Ca} is expected to be substantially smaller because divalent cations act as permeant blockers that reduce g_{ch} (Mak and Foskett, 1998; Mak et al., 2000). Despite their higher permeabilities, divalent cations bind strongly to site(s) in the channel pore so that they pass through the channel significantly more slowly than monovalent cations. In addition, the high $[K^+]$ in the cytoplasm and ER lumen (~ 140 mM) and the relatively weak selectivity of the $InsP_3R$ channel for Ca^{2+} over K^+ ($P_{Ca}:P_K = 15$) make K^+ a potentially effective competing

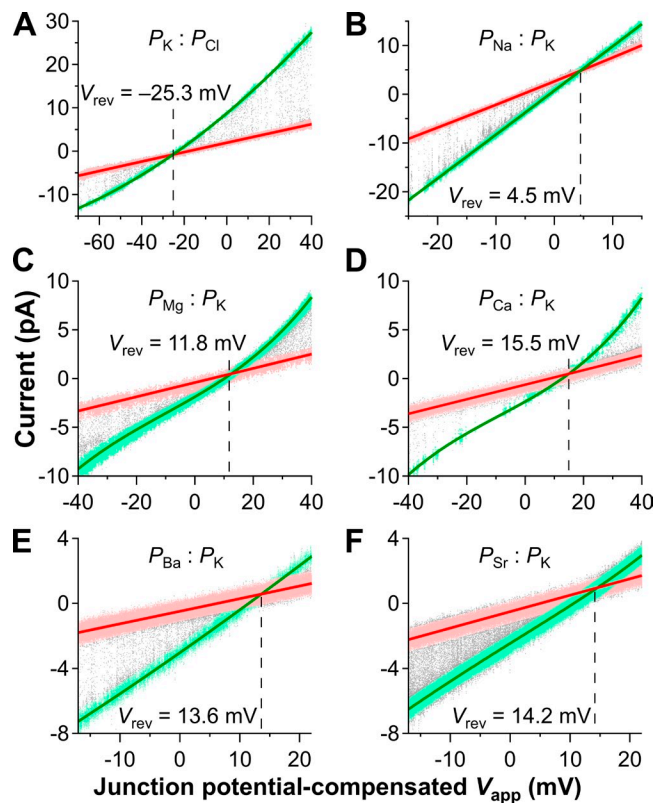


Figure 2. Representative I - V_{app} plots for single $InsP_3R$ -3 channels in excised lum-out nuclear membrane patches under asymmetric ionic conditions used to determine channel permeability ratios for various ions. Compositions of pipette and perfusion solutions are described in Materials and methods. Selected data points for I_{open} and I_{closed} are plotted in green and pink, respectively. Red lines are linear fits to I_{closed} - V_{app} data points, and green ones are polynomial fits to I_{open} - V_{app} data points (linear for B; quadratic for A, E, and F; cubic for C and D). V_{rev} at the intersection of the I_{open} - V_{app} and I_{closed} - V_{app} fits are marked by dashed lines and tabulated. (A) Eight V_{app} ramps in one of four experiments to determine $P_K:P_{Cl}$. Junction potential corrected ($V_{junction}$) = -9.3 ± 0.4 mV. (B) 15 V_{app} ramps in one of three experiments to determine $P_{Na}:P_K$. $V_{junction} = -1.5 \pm 0.2$ mV. (C) 10 V_{app} ramps in one of three experiments to determine $P_{Mg}:P_K$. $V_{junction} = -0.7 \pm 0.4$ mV. (D) 43 V_{app} ramps in one of three experiments to determine $P_{Ca}:P_K$. $V_{junction} = -1.4 \pm 0.2$ mV. (E) 35 V_{app} ramps in one of three experiments to determine $P_{Ba}:P_K$. $V_{junction} = -2.6 \pm 0.3$ mV. (F) 16 V_{app} ramps in one of three experiments to determine $P_{Sr}:P_K$. $V_{junction} = -2.2 \pm 0.8$ mV.

ion to also reduce i_{Ca} . i_{Ca} might be further reduced as a result of competition from free Mg^{2+} , which exists at significant levels ($\sim 200 \mu\text{M}$ – 1.1 mM) in both the cytoplasm and ER lumen (Halvorson et al., 1992; Morelle et al., 1994a,b; Silverman et al., 1994; Golding and Golding, 1995; Singh and Wisdom, 1995; Tashiro and Konishi, 1997), and has a permeability similar to that of Ca^{2+} ($P_{\text{Ca}}:P_{\text{Mg}} = 1.5$).

To measure i_{Ca} , we monitored the transmembrane current I through excised lum-out nuclear membrane patches containing a single active InsP_3R channel. The capability to switch the perfusion solutions around the excised patch was used to minimize systematic measurement errors by calibrating the patch clamp setup for each individual experiment. The lum-out membrane patch was first exposed to a perfusion solution with the same ionic composition as the pipette solution (symmetric ionic conditions). $I-V_{\text{app}}$ data were recorded with V_{app} ramped from -20 to 10 mV , and data points for $I_{\text{open}}-V_{\text{app}}$ and $I_{\text{closed}}-V_{\text{app}}$ were fitted linearly (Fig. 3 A). With no permeant ion concentration gradient across the excised nuclear membrane patch, the current passing through the InsP_3R channel ($I_{\text{open}}-I_{\text{closed}}$) and the leak current across the nuclear membrane patch (I_{closed}) must both be zero when $V_{\text{app}} = 0$. Thus, the intersection

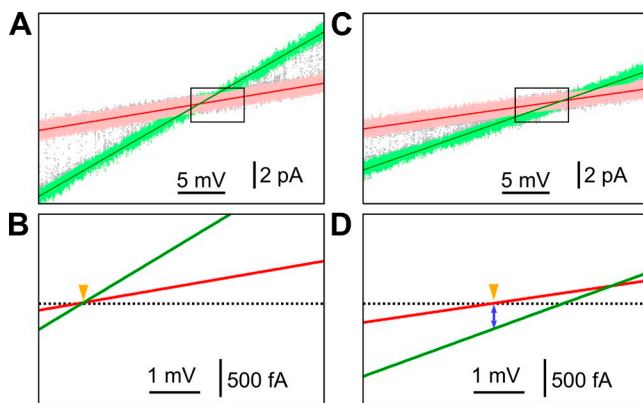


Figure 3. Measuring i_{Ca} in physiological ionic conditions. (A) Linear fits (green and red lines) to selected I_{open} and I_{closed} data (plotted in green and pink, respectively) from 25 V_{app} ramps recorded from an excised lum-out nuclear membrane patch containing one active InsP_3R channel under symmetric ionic conditions, with pipette and perfusion solutions containing 140 mM KCl , 0.5 mM MgCl_2 , and $3 \mu\text{M } [\text{Ca}^{2+}]_f$. Pipette solution contained $2 \mu\text{M } \text{InsP}_3$. (B) Graph of the fitted $I_{\text{open}}-V_{\text{app}}$ and $I_{\text{closed}}-V_{\text{app}}$ lines in the $I-V_{\text{app}}$ region marked by the black rectangle in A. Zero-current level (black dotted line) established at the intersection of the $I-V_{\text{app}}$ fits at $V_{\text{app}} = 0$ (marked by orange arrowhead). (C) Linear fits to I_{open} and I_{closed} data (same convention as in A) from 25 V_{app} ramps recorded for the same membrane patch under asymmetric ionic conditions, with perfusion solution containing 2 mM CaCl_2 . I and V_{app} ranges in A and C are the same. (D) Graph of the fitted $I-V_{\text{app}}$ lines in the same $I-V_{\text{app}}$ region with the same zero-current level as in B. $V_{\text{app}} = 0$ (marked by orange arrowhead) at the intersection of the $I_{\text{closed}}-V_{\text{app}}$ line and zero-current level. i_{Ca} is I_{open} at $V_{\text{app}} = 0$ (marked by blue arrow).

of the $I_{\text{open}}-V_{\text{app}}$ and $I_{\text{closed}}-V_{\text{app}}$ lines established the zero-current level for the patch clamp current recording system during each experiment (Fig. 3 B).

The perfusion solution was then switched to one with higher $[\text{Ca}^{2+}]_f$ (asymmetric ionic conditions). Higher $[\text{Ca}^{2+}]_{\text{ER}}$ reduced both the $\text{InsP}_3\text{R } g_{\text{ch}}$, as a result of an increase in permeant divalent cation block, and the leak conductance (Fig. 3 C). However, the zero-current level of the recording system was not affected by the perfusion solution switch. For the leak current (I_{closed}) through the excised membrane patch, $V_{\text{rev}} = 0$ because there are no significant concentration differences for the major ionic components in the pipette and perfusion solutions, K^+ and Cl^- , which have significantly higher mobility across the membrane than divalent cations (Beeler et al., 1981; Marhl et al., 1997). Therefore, $V_{\text{app}} = 0$ at the point where $I_{\text{closed}} = 0$ (Fig. 3 D). The open-channel current (I_{open}) at $V_{\text{app}} = 0$ is driven only by the $[\text{Ca}^{2+}]$ gradient across the channel ($\Delta[\text{Ca}^{2+}] = [\text{Ca}^{2+}]_{\text{ER}} - [\text{Ca}^{2+}]_i$) and therefore is i_{Ca} (Fig. 3 D).

We first measured i_{Ca} in symmetric 140 mM KCl with no Mg^{2+} . To cover the range of reported $[\text{Ca}^{2+}]_{\text{ER}}$ (Bygrave and Benedetti, 1996; Yu and Hinkle, 2000; Palmer et al., 2004), the luminal side of the excised membrane patch was exposed to perfusion solutions with $[\text{Ca}^{2+}]_f = 160 \mu\text{M}$, $550 \mu\text{M}$, and 1.1 mM . $[\text{Ca}^{2+}]_i$ in the pipette solution was fixed at $3 \mu\text{M}$ to keep channel P_o high. The observed magnitude of i_{Ca} was well described by a linear relation with $\Delta[\text{Ca}^{2+}]$ (Fig. 4), as predicted by the Goldman-Hodgkin-Katz current equation. However, the value for P_{Ca} ($1.5 \times 10^{-18} \text{ m}^3 \text{s}^{-1}$) derived from the slope of the i_{Ca} versus $\Delta[\text{Ca}^{2+}]$ line is an order of magnitude smaller than that ($1.5 \times 10^{-17} \text{ m}^3 \text{s}^{-1}$) estimated using g_{ch} in 140 mM

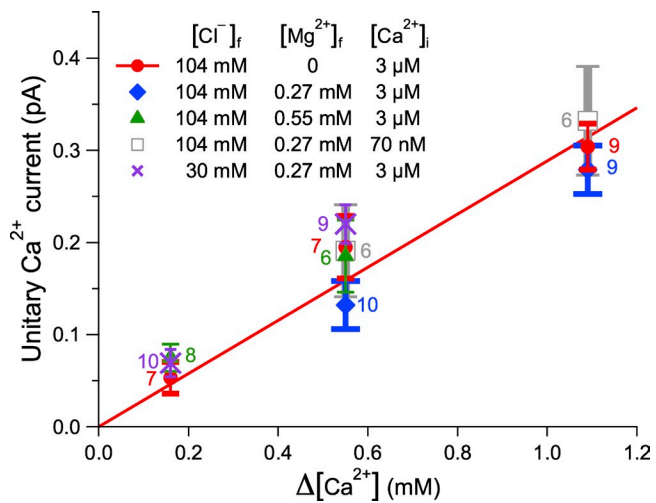


Figure 4. i_{Ca} 's through the InsP_3R channel under various asymmetric ionic conditions. Error bars show SEM. The number of measurements performed for each ionic condition is tabulated next to the corresponding data point. The line is the linear fit to the data points in 140 mM KCl , $0 \text{ mM } [\text{Mg}^{2+}]_f$, and $3 \mu\text{M } [\text{Ca}^{2+}]_i$, with slope of $0.30 \pm 0.02 \text{ pA/mM}$.

KCl and the measured permeability ratios of $P_{\text{Ca}}:P_{\text{K}}:P_{\text{Cl}}$. This discrepancy results from interactions between the channel and the permeant ions (K^+ and Ca^{2+}) and among permeant ions in the channel that are not considered in the Goldman-Hodgkin-Katz equation.

To assess the effect on i_{Ca} of physiological concentrations of free Mg^{2+} , ranging from 200 μM to 1.1 mM in both the cytoplasm and ER lumen (Halvorson et al., 1992; Morelle et al., 1994a,b; Silverman et al., 1994; Golding and Golding, 1995; Singh and Wisdom, 1995; Tashiro and Konishi, 1997), we measured i_{Ca} in symmetric 270 or 550 μM $[\text{Mg}^{2+}]_f$ with $[\text{Ca}^{2+}]_i = 3 \mu\text{M}$ and $[\text{Ca}^{2+}]_{\text{ER}} = 550 \mu\text{M}$ or 1.1 mM. Interestingly, i_{Ca} observed in the presence of physiological $[\text{Mg}^{2+}]_f$ was not significantly different from i_{Ca} measured in 0 $[\text{Mg}^{2+}]_f$ (Fig. 4).

Under normal physiological conditions, $[\text{Ca}^{2+}]_{\text{ER}}$ is significantly higher than $[\text{Ca}^{2+}]_i$, so i_{Ca} should have little dependence on $[\text{Ca}^{2+}]_i$. Indeed, we observed no statistical difference between i_{Ca} for $[\text{Ca}^{2+}]_i$ at resting (70 nM) and activating (3 μM) levels (Fig. 4).

Free chloride ion concentration $[\text{Cl}^-]_f$ is significantly lower than $[\text{K}^+]_f$ in the cytoplasm as a result of the Gibbs-Donnan effect of negative charges in cytoplasmic proteins (Foskett, 1990). To verify if physiological cytoplasmic $[\text{Cl}^-]_f$ significantly affects i_{Ca} , we measured i_{Ca} with pipette and perfusion solutions containing symmetric 100 mM potassium methanesulfonate (KCH_3SO_3), 40 mM KCl ($[\text{K}^+]_f \approx 104 \text{ mM}$, $[\text{Cl}^-]_f \approx 30 \text{ mM}$), and 270 μM $[\text{Mg}^{2+}]_f$, with $[\text{Ca}^{2+}]_i = 3 \mu\text{M}$ and $[\text{Ca}^{2+}]_{\text{ER}} = 550 \mu\text{M}$ or 1.1 mM. Again, i_{Ca} observed was not significantly different from that observed in 140 mM KCl (Fig. 4), indicating that i_{Ca} is to a large extent independent of $[\text{Cl}^-]_f$ under physiological ionic conditions. Interestingly, $g_{\text{ch}} = 293 \pm 4 \text{ pS}$ in symmetric 270 μM $[\text{Mg}^{2+}]_f$ and 30 mM $[\text{Cl}^-]_f$, the same as that observed in symmetric 270 μM $[\text{Mg}^{2+}]_f$ and 104 mM $[\text{Cl}^-]_f$ ($292 \pm 5 \text{ pS}$). This correspondence probably arises because decreasing $[\text{Cl}^-]_f$ reduces Cl^- current through the channel and also reduces Cl^- competition with K^+ to move through the channel, with the two opposing effects on InsP_3R g_{ch} cancelling each other out.

These results indicate that, in physiological ionic conditions, with symmetric 104 mM $[\text{K}^+]_f$, 30–104 mM $[\text{Cl}^-]_f$, 0–550 μM $[\text{Mg}^{2+}]_f$, 70 nM to 3 μM $[\text{Ca}^{2+}]_i$, the i_{Ca} for rat homotetrameric type 3 InsP_3R channel in native ER membrane is $(0.30 \pm 0.02 \text{ pA mM}^{-1}) \times [\text{Ca}^{2+}]_{\text{ER}}$. This is equivalent to having an asymptotic Ca^{2+} slope conductance (g_{ch} as V_{app} in the ER relative to the cytoplasm $\rightarrow \infty$) of $(23.4 \pm 1.6 \text{ pS mM}^{-1}) \times [\text{Ca}^{2+}]_{\text{ER}}$. For a filled store with 500 μM $[\text{Ca}^{2+}]_{\text{ER}}$, $i_{\text{Ca}} = 0.15 \pm 0.01 \text{ pA}$ and the asymptotic Ca^{2+} slope conductance is $11.7 \pm 0.8 \text{ pS}$.

Block of InsP_3R channel conduction by permeant divalent cations

Another indication of the inadequacy of the Goldman-Hodgkin-Katz equation to describe ionic flow through the InsP_3R channel is the substantial reduction of g_{ch} by

Ca^{2+} or Mg^{2+} (in millimolar concentrations) on the luminal or cytoplasmic side of the channel, despite their high permeability ratios (Fig. 5A). Similar partial reduction of g_{ch} by permeant divalent cations (Mg^{2+} , Ca^{2+} , and Ba^{2+}) was observed in endogenous type 1 InsP_3R channels in *Xenopus laevis* oocyte nuclear membrane (Mak and Foskett, 1998) and recombinant type 1 InsP_3R channels in the plasma membrane of DT40-KO-r- InsP_3R -1 cells (Dellis et al., 2006). This reduction suggests that movement of divalent cations through the InsP_3R channel is substantially slowed down by strong interactions between the ions and the pore, causing temporary block of ion flow through the channel (Hille, 2001). The channel conductance g_{ch} at the reversal potential V_{rev} was systematically evaluated in experiments performed to measure i_{Ca} in the presence of 3 μM , 160 μM , 550 μM , and 1.1 mM $[\text{Ca}^{2+}]_{\text{ER}}$, and symmetric 0, 270 μM and 550 μM $[\text{Mg}^{2+}]_f$. Channel blocking effects of Ca^{2+} and Mg^{2+} were not mutually exclusive, as the addition of Mg^{2+} further reduced g_{ch} already suppressed by Ca^{2+} , and vice versa (Fig. 5A). The observed reduction of g_{ch} by Ca^{2+} could be described by an empirical saturating partial inhibition equation:

$$g_{\text{ch}}([\text{Ca}^{2+}]_{\text{ER}}) = (g_{\infty\text{CaER}}[\text{Ca}^{2+}]_{\text{ER}} + g_0 K_{\text{CaER}}) / (K_{\text{CaER}} + [\text{Ca}^{2+}]_{\text{ER}}), \quad (2)$$

where g_0 is the channel slope conductance at 0 $[\text{Ca}^{2+}]_{\text{ER}}$, $g_{\infty\text{CaER}}$ is the channel slope conductance at saturating $[\text{Ca}^{2+}]_{\text{ER}}$, and K_{CaER} is the half-maximal blocking $[\text{Ca}^{2+}]_{\text{ER}}$. g_0 , $g_{\infty\text{CaER}}$, and K_{CaER} have different values in different $[\text{Mg}^{2+}]_f$ (corresponding to the different curves in Fig. 5A). In the absence of Mg^{2+} (Fig. 5A, red curve), $K_{\text{CaER}} = 210 \pm 20 \mu\text{M}$, $g_{\infty\text{CaER}} = 82 \pm 8 \text{ pS}$, and g_0 is 545 pS, the channel slope conductance with no divalent cations.

To compare the capacities of Mg^{2+} and Ca^{2+} to block the channel, we measured g_{ch} with various $[\text{Mg}^{2+}]_{\text{ER}}$, in 0 $[\text{Mg}^{2+}]_i$ and symmetric 3 μM $[\text{Ca}^{2+}]_f$ (Fig. 5B, purple open squares). g_{ch} data could be fitted using an equation similar to Eq. 2:

$$g_{\text{ch}}([\text{Mg}^{2+}]_{\text{ER}}) = (g_{\infty\text{MgER}}[\text{Mg}^{2+}]_{\text{ER}} + g_0 K_{\text{MgER}}) / (K_{\text{MgER}} + [\text{Mg}^{2+}]_{\text{ER}}). \quad (3)$$

Eq. 3 describes the purple curve in Fig. 5, with g_0 again being the channel conductance in the absence of divalent cations (545 pS). Interestingly, $g_{\infty\text{MgER}} = 81 \pm 5 \text{ pS}$ is very similar to $g_{\infty\text{CaER}}$, suggesting that Ca^{2+} and Mg^{2+} are equally efficacious in blocking the InsP_3R channel. Furthermore, $K_{\text{MgER}} = 410 \pm 20 \mu\text{M}$, which is $\approx 2 \times K_{\text{CaER}}$, suggesting that the affinity for Ca^{2+} of the site in the channel responsible for blockage by luminal divalent cations is twice that for Mg^{2+} ; i.e., Mg^{2+} is half as potent in blocking the InsP_3R channel as Ca^{2+} .

Although inhibition of InsP_3R gating by high $[\text{Ca}^{2+}]_i$ ($>20 \mu\text{M}$) (Mak et al., 2001b) prevents comparison of the effectiveness of Ca^{2+} from the cytoplasmic and luminal

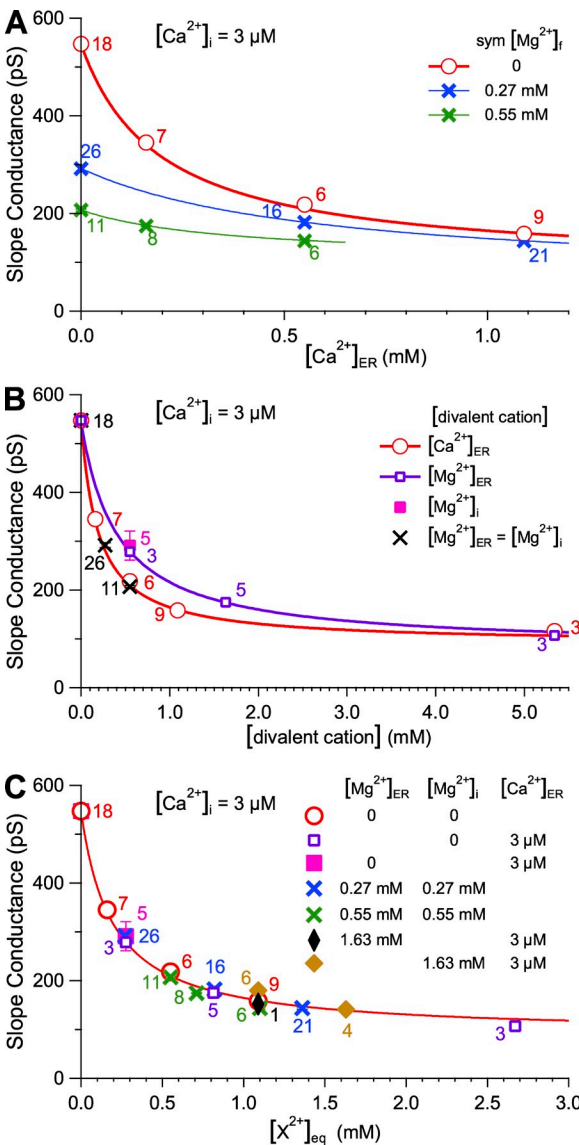


Figure 5. Slope conductance of an InsP₃R-3 channel at V_{rev} in symmetric 140-mM KCl solutions with various divalent cation concentrations. SEM for all data points are shown as error bars, some of which are smaller than the size of the symbols. The number of measurements performed for each ionic condition is tabulated next to the corresponding data point in the same color. The same symbols in the same color are used for the same set of data points plotted in the different graphs. (A) g_{ch} versus $[Ca^{2+}]_{ER}$ in the presence of various symmetric $[Mg^{2+}]_f$ as tabulated. Curves are fits to g_{ch} data by the empirical inhibition equation (Eq. 2), with different K_{CaER} for various $[Mg^{2+}]_f$. The red curve is for g_{ch} in 0 $[Mg^{2+}]_f$. (B) g_{ch} versus concentrations of divalent cations in the cytoplasmic or luminal side of the channel as tabulated. The purple curve is described by Eq. 3, and the red one is described by Eq. 5. (C) g_{ch} versus equivalent divalent cation concentrations $[X^{2+}]_{eq} = [Ca^{2+}]_{ER} + 0.5 \times ([Mg^{2+}]_i + [Mg^{2+}]_{ER})$ for various combinations of $[Ca^{2+}]_{ER}$, $[Mg^{2+}]_{ER}$, and $[Mg^{2+}]_i$ as tabulated. The red curve is described by Eq. 5.

sides to block permeation, the effectiveness of Mg²⁺ to block permeation from either side of the channel can be compared because physiological [Mg²⁺]_i has no significant effect on channel gating (Mak et al., 1999).

g_{ch} observed in 0.55 mM [Mg²⁺]_i and 0 [Mg²⁺]_{ER} (Fig. 5 B, magenta filled square) was the same as that in 0 [Mg²⁺]_i and 0.55 mM [Mg²⁺]_{ER}. This indicates that Mg²⁺ blocks the InsP₃R channel with equal potency from either side. Thus, the site responsible for permeant divalent cation block is probably located inside the pore along the ion permeation pathway, with cations from either side of the channel having similar access to the site.

The data for g_{ch} in symmetric $[Mg^{2+}]_f$ (Fig. 5 B, black crosses) fall on the curve described by Eq. 2 (Fig. 5 B, red curve), so that

$$g_{ch}([Mg^{2+}]_{sym}) = (g_{\infty CaER} [Mg^{2+}]_{sym} + g_0 K_{CaER}) / (K_{CaER} + [Mg^{2+}]_{sym}).$$

Using $g_{\infty CaER} = g_{\infty MgER} = g_{\infty}$, and $K_{CaER} = 0.5 K_{MgER}$,

$$g_{ch}([Mg^{2+}]_{sym}) = \frac{g_{\infty} ([Mg^{2+}]_{ER} + [Mg^{2+}]_i) + g_0 K_{MgER}}{K_{MgER} + ([Mg^{2+}]_{ER} + [Mg^{2+}]_i)}, \quad (4)$$

suggesting that contributions to channel block by Mg²⁺ on either side can be combined by simply summing the $[Mg^{2+}]_f$ on the two sides as if all the Mg²⁺ was on one side. This relation can even be extended to include $[Ca^{2+}]_{ER}$. g_{ch} data observed in various combinations of $[Ca^{2+}]_{ER}$, $[Mg^{2+}]_i$, and $[Mg^{2+}]_{ER}$ (whether $[Mg^{2+}]_i = [Mg^{2+}]_{ER}$ or not), when plotted against the equivalent divalent ion concentrations $[X^{2+}]_{eq}$ defined as $\{[Ca^{2+}]_{ER} + 0.5 \times ([Mg^{2+}]_{ER} + [Mg^{2+}]_i)\}$, are all well fitted by a curve similar to that described by Eq. 2 (Fig. 5 C, red curve); i.e.,

$$\begin{aligned} g_{ch}([Ca^{2+}]_{ER}, [Mg^{2+}]_{ER}, [Mg^{2+}]_i) \\ = \frac{g_{\infty} \{[Ca^{2+}]_{ER} + 0.5 \times ([Mg^{2+}]_{ER} + [Mg^{2+}]_i)\} + g_0 K_{CaER}}{K_{CaER} + \{[Ca^{2+}]_{ER} + 0.5 \times ([Mg^{2+}]_{ER} + [Mg^{2+}]_i)\}} \\ = \frac{g_{\infty} [X^{2+}]_{eq} + g_0 K_{CaER}}{K_{CaER} + [X^{2+}]_{eq}}. \end{aligned} \quad (5)$$

This result strongly indicates that channel block by different permeant divalent cations is caused by binding to a unique, saturable site in the ion permeation pathway that is equally accessible from either side of the channel, with an affinity for Ca²⁺ twice that for Mg²⁺. This site is probably located at or near the selectivity filter of the channel where the channel pore size is most restricted.

DISCUSSION

Magnitude of i_{Ca} through the InsP₃R channel in physiological ionic conditions

In this study, the conduction properties of a homotetrameric recombinant rat InsP₃R-3 channel were examined

under various ionic conditions, especially under physiological monovalent and divalent ion concentrations. Under physiological ranges of $[K^+]_f$, $[Cl^-]_f$, $[Mg^{2+}]_f$, $[Ca^{2+}]_i$, and $[Ca^{2+}]_{ER}$, i_{Ca} through an open $InsP_3R$ channel depends only on $[Ca^{2+}]_{ER}$ with a linear relation. $i_{Ca} = 0.15 \pm 0.01$ pA for a filled ER store with 500 μM $[Ca^{2+}]_{ER}$. This value is compatible with the magnitude of Ca^{2+} flux estimated by the imaging of Ca^{2+} release events (puffs) of 0.4–2.5 pA (Sun et al., 1998) and 0.12–0.95 pA (Bruno et al., 2010) in *Xenopus* oocytes, where multiple active $InsP_3R$ channels were involved in generating a puff. The value is also in reasonable agreement with the values for i_{Ca} estimated from Ca^{2+} release events (blips and puffs): ~ 0.4 pA (Shuai et al., 2006) and ~ 0.1 pA (Bruno et al., 2010) for endogenous $InsP_3R$ -1 in *Xenopus* oocytes, and ~ 0.05 pA i_{Ca} estimated for endogenous $InsP_3R$ -1 channels in human neuroblastoma SH-SY5Y cells (Smith and Parker, 2009). Accordingly, our experimental approach, with the advantages of observing Ca^{2+} currents with single-channel resolution and rigorous control of ionic conditions on both sides of the channel, appears to accurately reflect the physiological behavior of $InsP_3R$ channels in intact cells. Furthermore, our measured value of i_{Ca} is comparable to the i_{Ca} of 0.1 pA (Swillens et al., 1999), 0.07 pA (Thul and Falcke, 2004), and 0.2 pA (Shuai et al., 2008), assumed in various efforts to numerically simulate Ca^{2+} release through $InsP_3R$ channels, thus providing experimental support for the validity of those modeling efforts.

i_{Ca} for $InsP_3R$ measured here is comparable to but smaller than those determined for RYR channels, the other major family of intracellular Ca^{2+} release channels. i_{Ca} driven by 500 μM $[Ca^{2+}]_{ER}$ through purified amphibian type 1 RYR (RYR1) and mammalian type 2 RYR (RYR2) channels reconstituted in artificial lipid bilayers was estimated to be 0.26 and 0.27 pA, respectively, in the presence of symmetric 150 mM KCl and 1 mM $MgCl_2$ (Kettlun et al., 2003). Under similar ionic conditions (140 mM KCl and 1 mM $MgCl_2$), i_{Ca} through an open rat $InsP_3R$ -3 channel is 0.15 pA. However, as discussed in more detail below, if the lipid environment impinges on the conductance properties of the release channels, a comparison of the i_{Ca} may not yet be possible because i_{Ca} measurements for the two channel types were obtained in different membrane environments.

$InsP_3R$ channel conductance

g_{ch} of various $InsP_3R$ channel isoforms in symmetric 140 mM KCl has been observed, mainly by nuclear patch clamp experiments (Mak and Foskett, 1998; Mak et al., 2000; Boehning et al., 2001a; Ionescu et al., 2006; Betzenhauser et al., 2009), to be comparable to but smaller than those for RYR channels reconstituted into lipid bilayers under the same KCl concentration: ~ 750 pS for RYR1 (Wang et al., 2005) and 740 pS for RYR2

(Lindsay et al., 1991). Comparisons of primary sequences of different $InsP_3R$ isoforms from various species with those of RYR isoforms reveal that a conserved sequence GGGXGDX (amino acid residues 2545–2551 in rat $InsP_3R$ -1 SII⁺ SII⁺ isoform [Mignery et al., 1990] and 2472–2478 in rat $InsP_3R$ -3 [Blondel et al., 1993]; X stands for I or V) between putative transmembrane helices 5 and 6 in the $InsP_3R$ pore-forming domain is highly homologous to the sequence GGGIGDE (amino acid residues 4895–4901 in human RYR1 [Fujii et al., 1991] and 4824–4830 in human RYR2 [Zorzato et al., 1990]), which is conserved in all three RYR isoforms. Site-directed mutagenesis in the homologous RYR sequence alters the conductance properties of RYR channels (Zhao et al., 1999; Gao et al., 2000; Du et al., 2001; Chen et al., 2002; Wang et al., 2005), suggesting that those amino acids lie in or near the selectivity filter that determines, at least in part, the conductance of the RYR channel. Point mutations in the corresponding sequence in the rat $InsP_3R$ -1 also altered its conductance properties (Boehning et al., 2001b). A mutation changing the GGGVGDV sequence to GGGIGDV made it more similar to that of the RYR and increased $InsP_3R$ channel conductance (Boehning et al., 2001b). Conversely, GGGIGDE to GGGVGDE (Gao et al., 2000) and GGGIGDE to GGGIGDQ (Wang et al., 2005) substitutions in the RYR sequence generated channels with reduced conductance. Furthermore, invertebrate $InsP_3R$ isoforms have a GGGIGDI sequence (Yoshikawa et al., 1992; Baylis et al., 1999; Iwasaki et al., 2002) that resembles the RYR sequence and have a higher single-channel conductance (477 ± 3 pS; Ionescu et al., 2006) than the vertebrate isoforms ($360 - 390$ pS; Mak and Foskett, 1998; Mak et al., 2000; Boehning et al., 2001a; Betzenhauser et al., 2009), which have a GGGVGDX sequence. Collectively, these observations strongly suggest that the GGGXGDX sequence in $InsP_3R$ is close to or forms part of the selectivity filter in the tetrameric channel, and is therefore a major factor that determines the conductance properties of $InsP_3R$ channels. However, mutagenesis suggests that amino acids outside the GGGXGDX sequence also play a role in determining the conductance of the $InsP_3R$ (unpublished data) and RYR (Gao et al., 2000; Du et al., 2001; Xu et al., 2006) channels, possibly through electrostatic effects to concentrate ions in the channel.

Other factors also appear to contribute to the channel conductance properties. Different single-channel conductances have been observed for the same recombinant $InsP_3R$ -1 isoform expressed in DT40- $InsP_3R$ -KO cells, depending on whether it was localized in the outer nuclear membrane (373 ± 2 pS; Betzenhauser et al., 2009) or the plasma membrane (214 ± 17 pS; Delliis et al., 2006). Moreover, the conductance of the homotetrameric recombinant $InsP_3R$ -3 channel expressed in the outer nuclear envelope of DT40-KO-r- $InsP_3R$ -3 cells

measured here (545 ± 7 pS) is nearly 50% larger than that observed for the same recombinant InsP_3R -3 channel expressed in the outer nuclear envelope of *Xenopus* oocytes (370 ± 8 pS; Mak et al., 2000). Conductance values (~ 125 and 200 pS) smaller than the one we observed here were reported for the same channel in the same location from the same cell type (Taufiq-Ur-Rahman et al., 2009), but those smaller and variable conductances were likely a result of heavy contamination by Mg^{2+} of the Na_2ATP used (Rahman and Taylor, 2009). The conductance of the r- InsP_3R -3 channels in the outer nuclear membrane of DT40-KO-r- InsP_3R -3 cells is even larger than that for the invertebrate InsP_3R (477 ± 3 pS; Ionescu et al., 2006), despite the more RYR-like putative selectivity filter sequence of the latter. Because all of these patch clamp studies of various InsP_3R channels were all performed in symmetric 140 mM KCl ($[\text{K}^+]_f = 104$ mM), these observations suggest that besides the primary sequences of the InsP_3R , other factor(s)—lipid environment, interacting proteins or peptides, etc., that are different in various expression systems (outer nuclear membrane vs. plasma membrane; DT40-KO-r- InsP_3R -3 nucleus vs. *Xenopus* oocyte nucleus)—can affect the conductance of InsP_3R channels substantially.

The factors that cause the differences of the InsP_3R -3 g_{ch} observed in the same rigorously controlled ionic conditions (symmetric 140 mM KCl) in different cellular locations and different cells may also affect the size of i_{Ca} through InsP_3R -3 channels in those contexts. Because ours is the first measurement of i_{Ca} through an InsP_3R channel under physiological ionic conditions, how i_{Ca} correlates with g_{ch} in various cell systems cannot be clearly gauged until similar measurements are made in different systems. It should be pointed out that although the ionic conditions ($[\text{Ca}^{2+}]_{\text{ER}}$, $[\text{Mg}^{2+}]_f$, $[\text{K}^+]$, and $[\text{Cl}^-]$) under which i_{Ca} was measured in this study were physiological or near-physiological, the ionic conditions under which g_{ch} in symmetric 140 mM KCl were measured (in this study and all published reports) were nonphysiological because of the absence of divalent cations, especially Mg^{2+} , on either side of the channels. It is possible that the observed variability of g_{ch} is a result of the use of nonphysiological ionic conditions, as a study on the effects of divalent cations on InsP_3R g_{ch} suggested (Mak and Foskett, 1998). This issue can be clarified with more direct measurements of i_{Ca} for other InsP_3R channels in different cell systems. At this point, the applicability of the i_{Ca} of homotetrameric type 3 InsP_3R channels in DT40-KO-r- InsP_3R -3 cells to other InsP_3R channels and cell types should be considered judiciously with recognition of its potential limits. However, this first direct measurement is of significant value for improving our understanding of the mechanisms of InsP_3R -mediated Ca^{2+} release and for modeling efforts to simulate Ca^{2+} signaling.

Selective permeant ion block of the InsP_3R channel by Mg^{2+}

Physiological $[\text{Mg}^{2+}]_f$ (200 μM – 1.1 mM in both the cytoplasm and ER lumen) substantially reduced g_{ch} of the InsP_3R channel in symmetric 140 -mM KCl solutions (Fig. 5) by acting as a permeant blocking cation. This indicates that under physiological conditions, Mg^{2+} significantly affects the passage of K^+ through the InsP_3R channel pore. Accordingly, it is not immediately obvious why i_{Ca} was not measurably different in the presence or absence of physiological $[\text{Mg}^{2+}]_f$ (Fig. 4). Similarly, i_{Ca} 's passing through RYR channels under physiological (~ 500 μM) $[\text{Ca}^{2+}]_{\text{ER}}$ (Chen et al., 2003; Kettun et al., 2003; Gillespie and Fill, 2008) were not significantly affected by the presence or absence of 1 mM MgCl_2 .

Because of the lack, to date, of a quantitative model to describe the conductance properties of the InsP_3R channel pore, we attempt to explain qualitatively the apparently contradicting observations by using models developed to account for conductance properties of RYR channels, which have a putative selectivity filter sequence, and therefore structure, highly homologous to those of InsP_3R channels.

In a barrier model that describes the RYR channel as a single-ion occupancy channel with four energy barriers in the selectivity filter (Tinker et al., 1992), the channel is blocked when any cation enters the vacant selectivity filter because the channel cannot accommodate two cations simultaneously. Despite higher permeability of Mg^{2+} than K^+ , because $[\text{K}^+]_f$ in the cytoplasm and ER lumen is about two orders of magnitude higher than $[\text{Mg}^{2+}]_f$, K^+ is likely to be the major permeant blocker of i_{Ca} through the InsP_3R channel. Furthermore, because of the higher affinity of Ca^{2+} for the selectivity filter relative to that of Mg^{2+} , as revealed by its more potent reduction of InsP_3R g_{ch} (Fig. 5), the energy released as Ca^{2+} enters the channel selectivity filter from the luminal side can compensate for the energy required to push an occupying Mg^{2+} out the cytoplasmic side, especially if the Mg^{2+} is bound to the side energy well close to the cytoplasmic end of the filter. Thus, it is possible that the i_{Ca} through the InsP_3R channel is already significantly suppressed by physiological $[\text{K}^+]_f$, such that Mg^{2+} , with lower affinity for the selectivity filter than Ca^{2+} , cannot reduce the magnitude of i_{Ca} further by a detectable amount.

In Poisson-Nernst Planck models with (Gillespie et al., 2005) and without (Chen et al., 1997, 2003) density function theory, a cation-selective channel is described as one with a constricted selectivity filter region containing negative charges from acidic amino side chains or carbonyl backbones. Cations move through the pore by electrodiffusion under electrical and concentration gradients, interacting with the channel both electrostatically and chemically. According to these models, concentrations of cations in the selectivity filter of the

RYR/InsP₃R channel are higher than those in the bulk solutions because of the permanent negative charges from the Asp (in GGGXGDX in InsP₃R) or Asp and Glu (GGGIGDE in RYR) located in or near the selectivity filter of the channel. This concentrating effect is stronger for Ca²⁺ and Mg²⁺ than for K⁺ because of the more negative chemical potentials of Ca²⁺ and Mg²⁺ in the selectivity filter as a result of either chemical interactions between the divalent cations and the channel (Chen et al., 2003), or because of the smaller ionic radii and therefore smaller excluded volumes and higher charge densities of Ca²⁺ and Mg²⁺ (Gillespie, 2008). The high divalent cation concentration in or near the selectivity filter in turn lowers [K⁺] there as a result of electrostatic repulsion between the cations (Chen et al., 2003; Gillespie et al., 2005; Gillespie, 2008). This can cause the observed reduction of g_{ch} by physiological concentrations of Mg²⁺ or Ca²⁺. In InsP₃R channels, the conserved sequence GGGXGDX in or near the selectivity filter has fewer acidic residues than the corresponding sequence GGGIGDE for the RYR channels. This may reduce the permanent negative charge density in the InsP₃R channel selectivity filter relative to that for the RYR channel and consequently weaken the electrostatic interaction between the selectivity filter and the cations (Gillespie et al., 2005), making the effect of the more negative chemical potential of Ca²⁺ than Mg²⁺ in the filter even more prominent in the InsP₃R than RYR, as indicated by the substantial higher potency of Ca²⁺ than Mg²⁺ to reduce InsP₃R g_{ch} (Fig. 5). High [Ca²⁺]_f in the InsP₃R selectivity filter will suppress entry of Mg²⁺ through electrostatic repulsion. With only physiological [Mg²⁺]_f in the bulk solution around the channel, there may not be enough Mg²⁺ in the filter to significantly impede the flux of Ca²⁺.

[Ca²⁺]_i at various distances from an open InsP₃R channel as a result of i_{Ca}

The size of i_{Ca} through an open InsP₃R channel in the ER membrane obviously directly affects the [Ca²⁺]_i immediately surrounding it. Measurement of i_{Ca} in physiological ionic conditions now enables us to estimate the [Ca²⁺]_i in the vicinity of an open InsP₃R. For the estimation, the channel pore can be treated as a point source in a semi-infinite region (Smith, 1996). Within short distances from the open-channel pore (<15 nm), the concentrations and Ca²⁺-binding rates of endogenous cytoplasmic Ca²⁺ buffers are too low to significantly affect the local [Ca²⁺]_i. Thus, local [Ca²⁺]_i in the immediate vicinity of the open channel is mainly determined by the equilibrium between Ca²⁺ flux through the channel and diffusion of unbound Ca²⁺ through the cytosol, and can be estimated with reasonable accuracy as

$$[Ca^{2+}]_i(r) \approx [i_{Ca} / (z_{Ca} F 2\pi D r)] \approx 1.1 \times [Ca^{2+}]_{ER} nm / r, \quad (6)$$

where r is the distance from the channel pore, D is the diffusion coefficient for Ca²⁺ in the cytoplasm with no buffering, and z_{Ca} and F are as defined in Eq. 1 (Smith, 1996; Neher, 1998), using the value of i_{Ca} measured here and $D \approx 225 \mu m^2 s^{-1}$ (Allbritton et al., 1992). According to cryo-electron microscopy (Jiang et al., 2002; da Fonseca et al., 2003; Hamada et al., 2003; Serysheva et al., 2003; Sato et al., 2004; Wolfram et al., 2010) and electron microscopy (Cárdenas et al., 2010a) measurements, the radius of a tetrameric InsP₃R channel in a plane perpendicular to the axis of the channel pore is $\sim 10-12$ nm. There is no structural information concerning the locations of various Ca²⁺-binding sites in the channel relative to the pore, but it is reasonable to assume that the distance between the sites and the pore is $< 10-12$ nm. Using 8 nm as an estimate of the distance between the channel pore and the activating and inhibitory Ca²⁺-binding sites of the channel, within the physiological range of [Ca²⁺]_{ER} (100–500 μM), [Ca²⁺]_i is sensed by the channel; i.e., [Ca²⁺]_i (8 nm) $\approx 14-69 \mu M$ (Fig. 6). This [Ca²⁺]_i level is reached within a short time (microsecond) after the opening of the channel (Neher, 1998). With a filled ER store, [Ca²⁺]_i (8 nm) is high enough that even at saturating [InsP₃], P_o of the open channel itself is significantly inhibited for most InsP₃R isoforms that have been studied in single-channel experiments (Foskett et al., 2007). This can provide negative feedback to terminate the Ca²⁺ release. On the other hand, when the ER store is partially depleted, Ca²⁺ released by the InsP₃R channel may not be sufficient to raise [Ca²⁺]_i high enough to suppress activity of the releasing channel to terminate the Ca²⁺ release.

Farther away from the channel pore, [Ca²⁺]_i is strongly affected by cytoplasmic Ca²⁺ buffers. Estimates of concentrations and Ca²⁺-binding rates of endogenous Ca²⁺

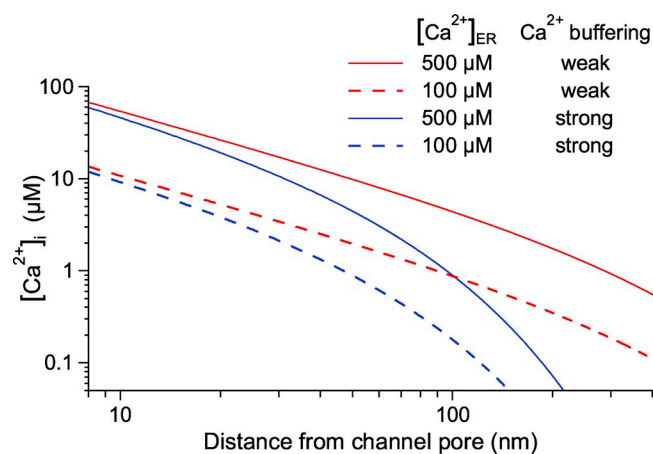


Figure 6. Spatial profiles of [Ca²⁺]_i at various distances from an open InsP₃R channel for different [Ca²⁺]_{ER} with different cytoplasmic Ca²⁺-buffering capacities. [Ca²⁺]_i was calculated using Eq. 7 with characteristic length $\lambda = 55$ and 440 nm for strong and weak cytoplasmic Ca²⁺ buffering, respectively.

buffer(s) (B_T and k_{on} , respectively) vary widely (Wagner and Keizer, 1994; Smith et al., 1996; Falcke, 2003; Shuai et al., 2008), so only a first-order estimate of $[Ca^{2+}]_i(r)$ is feasible for a general case. For simplicity, so that $[Ca^{2+}]_i(r)$ can be evaluated analytically, the excess buffer approximation is assumed (Smith, 1996) for our rough estimation, so

$$[Ca^{2+}]_i(r) \approx [i_{Ca} / (z_{Ca} F 2\pi D r)] \exp(-r/\lambda), \quad (7)$$

where λ , the characteristic length, is $(D/k_{on}B_T)^{1/2}$. From parameters used in Wagner and Keizer (1994), Smith et al. (1996), and Falcke (2003), we determined a high and low estimate for λ as 440 and 55 nm, respectively, and estimated the range of $[Ca^{2+}]_i(r)$ using Eq. 7 (Fig. 6).

For $r > 200$ nm, $[Ca^{2+}]_i(r)$ calculated from the two estimates for λ differs by over two orders of magnitude (Fig. 6), and it is no longer meaningful to consider $[Ca^{2+}]_i(r)$ for a general case. More specific values for k_{on} and B_T are needed to give a better evaluation of $[Ca^{2+}]_i$.

From our estimation, it is clear that as $[Ca^{2+}]_i(r)$ decreases for larger r , there is a range of r within which the Ca^{2+} released by an open $InsP_3R$ channel can activate a neighboring channel at that distance away, as long as $[InsP_3]$ is sufficiently elevated, for all $InsP_3Rs$ studied (Foskett et al., 2007). Thus, the magnitude of i_{Ca} observed confirms that CICR can be a mechanism to couple neighboring $InsP_3R$ channels to coordinate concerted Ca^{2+} release by multiple channels to generate various intracellular Ca^{2+} signals.

In this simple consideration, the $[Ca^{2+}]_i$ profile was estimated around an open channel with $P_o = 1$. In reality, the amount of Ca^{2+} moving through the releasing channel depends not only on i_{Ca} , but also on the stochastic gating of the releasing channel, which is dynamically regulated by the local $[InsP_3]$ and $[Ca^{2+}]_i$ (Foskett et al., 2007), which in turn are affected by Ca^{2+} released by the releasing channel and any neighboring active channels. Furthermore, the activation of an $InsP_3R$ channel by CICR is a complex dynamic process regulated by stochastic binding and unbinding of $InsP_3$ and Ca^{2+} to activating and inhibitory sites, which are affected not only by local $[Ca^{2+}]_i$, but also by the on- and off-rates of the sites that can be allosterically coupled (Atri et al., 1993; Tang et al., 1996; Kaftan et al., 1997; Moraru et al., 1999; Dawson et al., 2003; Mak et al., 2003). To properly take into consideration all of these complicated factors affecting the regulation of Ca^{2+} signaling, quantitative kinetic modeling (De Young and Keizer, 1992; Swillens et al., 1994, 1998, 1999; Dupont and Swillens, 1996; Tang et al., 1996; Falcke et al., 2000; Sneyd and Falcke, 2005; Swaminathan et al., 2009) using the right parameters, of which i_{Ca} is a critical one, is necessary.

In summary, we have described the first direct electrophysiological measurements of the i_{Ca} 's driven by physiological $[Ca^{2+}]$ gradients across single $InsP_3R$ channels

in a native ER membrane environment under physiological ionic conditions. These measurements will enable more accurate evaluations of the amount of Ca^{2+} released in a fundamental Ca^{2+} release event mediated by a single $InsP_3R$ channel, contribute to a better estimation of the coupling between the activities of neighboring $InsP_3R$ channels through CICR, and provide insights to improve future understanding and modeling of intracellular Ca^{2+} signals.

We thank John E. Pearson for helpful discussions.

This work was supported by National Institutes of Health grants R01 GM074999 (to D.-O.D. Mak), R01 GM065830 (to D.-O.D. Mak and J.K. Foskett), and R01 MH059937 to (J.K. Foskett).

Richard L. Moss served as editor.

Submitted: 9 August 2010

Accepted: 21 October 2010

REFERENCES

Allbritton, N.L., T. Meyer, and L. Stryer. 1992. Range of messenger action of calcium ion and inositol 1,4,5-trisphosphate. *Science*. 258:1812–1815. doi:10.1126/science.1465619

Atri, A., J. Amundson, D. Clapham, and J. Sneyd. 1993. A single-pool model for intracellular calcium oscillations and waves in the *Xenopus laevis* oocyte. *Biophys. J.* 65:1727–1739. doi:10.1016/S0006-3495(93)81191-3

Baylis, H.A., T. Furuchi, F. Yoshikawa, K. Mikoshiba, and D.B. Sattelle. 1999. Inositol 1,4,5-trisphosphate receptors are strongly expressed in the nervous system, pharynx, intestine, gonad and excretory cell of *Caenorhabditis elegans* and are encoded by a single gene (itr-1). *J. Mol. Biol.* 294:467–476. doi:10.1006/jmbi.1999.3229

Beeler, T.J., R.H. Farmen, and A.N. Martonosi. 1981. The mechanism of voltage-sensitive dye responses on sarcoplasmic reticulum. *J. Membr. Biol.* 62:113–137. doi:10.1007/BF01870205

Berridge, M.J. 1993. Inositol trisphosphate and calcium signalling. *Nature*. 361:315–325. doi:10.1038/361315a0

Berridge, M.J. 1997. Elementary and global aspects of calcium signalling. *J. Physiol.* 499:291–306.

Berridge, M.J., P. Lipp, and M.D. Bootman. 2000. The versatility and universality of calcium signalling. *Nat. Rev. Mol. Cell Biol.* 1:11–21. doi:10.1038/35036035

Betzenhauser, M.J., L.E. Wagner II, H.S. Park, and D.I. Yule. 2009. ATP regulation of type-1 inositol 1,4,5-trisphosphate receptor activity does not require Walker A-type ATP-binding motifs. *J. Biol. Chem.* 284:16156–16163. doi:10.1074/jbc.M109.006452

Bezprozvanny, I., and B.E. Ehrlich. 1995. The inositol 1,4,5-trisphosphate ($InsP_3$) receptor. *J. Membr. Biol.* 145:205–216.

Blondel, O., J. Takeda, H. Janssen, S. Seino, and G.I. Bell. 1993. Sequence and functional characterization of a third inositol trisphosphate receptor subtype, IP_3R-3 , expressed in pancreatic islets, kidney, gastrointestinal tract, and other tissues. *J. Biol. Chem.* 268:11356–11363.

Boehning, D., S.K. Joseph, D.-O.D. Mak, and J.K. Foskett. 2001a. Single-channel recordings of recombinant inositol trisphosphate receptors in mammalian nuclear envelope. *Biophys. J.* 81:117–124. doi:10.1016/S0006-3495(01)75685-8

Boehning, D., D.-O.D. Mak, J.K. Foskett, and S.K. Joseph. 2001b. Molecular determinants of ion permeation and selectivity in inositol 1,4,5-trisphosphate receptor Ca^{2+} channels. *J. Biol. Chem.* 276:13509–13512.

Bootman, M.D., M.J. Berridge, and P. Lipp. 1997. Cooking with calcium: the recipes for composing global signals from elementary events. *Cell*. 91:367–373. doi:10.1016/S0092-8674(00)80420-1

Bootman, M.D., T.J. Collins, C.M. Peppiatt, L.S. Prothero, L. MacKenzie, P. De Smet, M. Travers, S.C. Tovey, J.T. Seo, M.J. Berridge, et al. 2001. Calcium signalling—an overview. *Semin. Cell Dev. Biol.* 12:3–10. doi:10.1006/scdb.2000.0211

Braet, K., L. Cabooter, K. Paemeleire, and L. Leybaert. 2004. Calcium signal communication in the central nervous system. *Biol. Cell*. 96:79–91. doi:10.1016/j.biocel.2003.10.007

Bruno, L., G. Solovey, A.C. Ventura, S. Dargan, and S.P. Dawson. 2010. Quantifying calcium fluxes underlying calcium puffs in *Xenopus laevis* oocytes. *Cell Calcium*. 47:273–286. doi:10.1016/j.ceca.2009.12.012

Butler, J.N. 1968. The thermodynamic activity of calcium ion in sodium chloride-calcium chloride electrolytes. *Biophys. J.* 8:1426–1433. doi:10.1016/S0006-3495(68)86564-6

Bygrave, F.L., and A. Benedetti. 1996. What is the concentration of calcium ions in the endoplasmic reticulum? *Cell Calcium*. 19:547–551. doi:10.1016/S0143-4160(96)90064-0

Cárdenas, C., M. Escobar, A. García, M. Osorio-Reich, S. Härtel, J.K. Foskett, and C. Franzini-Armstrong. 2010a. Visualization of inositol 1,4,5-trisphosphate receptors on the nuclear envelope outer membrane by freeze-drying and rotary shadowing for electron microscopy. *J. Struct. Biol.* 171:372–381. doi:10.1016/j.jsb.2010.05.003

Cárdenas, C., R.A. Miller, I. Smith, T. Bui, J. Molgó, M. Müller, H. Vais, K.H. Cheung, J. Yang, I. Parker, et al. 2010b. Essential regulation of cell bioenergetics by constitutive InsP₃ receptor Ca²⁺ transfer to mitochondria. *Cell*. 142:270–283. doi:10.1016/j.cell.2010.06.007

Chen, D.P., L. Xu, A. Tripathy, G. Meissner, and B. Eisenberg. 1997. Permeation through the calcium release channel of cardiac muscle. *Biophys. J.* 73:1337–1354. doi:10.1016/S0006-3495(97)78167-0

Chen, D.P., L. Xu, B. Eisenberg, and G. Meissner. 2003. Calcium ion permeation through the calcium release channel (ryanodine receptor) of cardiac muscle. *J. Phys. Chem. B*. 107:9139–9145. doi:10.1021/jp0354191

Chen, S.R.W., P. Li, M. Zhao, X. Li, and L. Zhang. 2002. Role of the proposed pore-forming segment of the Ca²⁺ release channel (ryanodine receptor) in ryanodine interaction. *Biophys. J.* 82:2436–2447. doi:10.1016/S0006-3495(02)75587-2

Clapham, D.E. 1995. Calcium signaling. *Cell*. 80:259–268. doi:10.1016/0092-8674(95)90408-5

da Fonseca, P.C., S.A. Morris, E.P. Nerou, C.W. Taylor, and E.P. Morris. 2003. Domain organization of the type 1 inositol 1,4,5-trisphosphate receptor as revealed by single-particle analysis. *Proc. Natl. Acad. Sci. USA*. 100:3936–3941. doi:10.1073/pnas.0536251100

Dawson, A.P., E.J. Lea, and R.F. Irvine. 2003. Kinetic model of the inositol trisphosphate receptor that shows both steady-state and quantal patterns of Ca²⁺ release from intracellular stores. *Biochem. J.* 370:621–629. doi:10.1042/BJ20021289

De Young, G.W., and J. Keizer. 1992. A single-pool inositol 1,4,5-trisphosphate-receptor-based model for agonist-stimulated oscillations in Ca²⁺ concentration. *Proc. Natl. Acad. Sci. USA*. 89:9895–9899. doi:10.1073/pnas.89.20.9895

Dellis, O., S.G. Dedos, S.C. Tovey, S.J. Taufiq-Ur-Rahman, S.J. Dubel, and C.W. Taylor. 2006. Ca²⁺ entry through plasma membrane IP₃ receptors. *Science*. 313:229–233. doi:10.1126/science.1125203

Du, G.G., X. Guo, V.K. Khanna, and D.H. MacLennan. 2001. Functional characterization of mutants in the predicted pore region of the rabbit cardiac muscle Ca²⁺ release channel (ryanodine receptor isoform 2). *J. Biol. Chem.* 276:31760–31771. doi:10.1074/jbc.M102751200

Dupont, G., and S. Swillens. 1996. Quantal release, incremental detection, and long-period Ca²⁺ oscillations in a model based on regulatory Ca²⁺-binding sites along the permeation pathway. *Biophys. J.* 71:1714–1722. doi:10.1016/S0006-3495(96)79373-6

Falcke, M. 2003. Buffers and oscillations in intracellular Ca²⁺ dynamics. *Biophys. J.* 84:28–41. doi:10.1016/S0006-3495(03)74830-9

Falcke, M., L. Tsimring, and H. Levine. 2000. Stochastic spreading of intracellular Ca²⁺ release. *Phys. Rev. E Stat. Phys. Plasmas Fluids Relat. Interdiscip. Topics*. 62:2636–2643.

Foskett, J.K. 1990. Optical studies of ion and water transport. In *Noninvasive Techniques in Cell Biology*. J.K. Foskett and S. Grinstein, editors. Wiley-Liss, New York. 237–272.

Foskett, J.K., and D.-O.D. Mak. 2010. Regulation of IP₃R channel gating by Ca²⁺ and Ca²⁺ binding proteins. In *Current Topics in Membranes Vol. 66: Structure-Function of Ca²⁺ Release Channels*. I.I. Serysheva, editor. Elsevier, Amsterdam. 235–272.

Foskett, J.K., C. White, K.H. Cheung, and D.-O.D. Mak. 2007. Inositol trisphosphate receptor Ca²⁺ release channels. *Physiol. Rev.* 87:593–658. doi:10.1152/physrev.00035.2006

Fujii, J., K. Otsu, F. Zorzato, S. de Leon, V.K. Khanna, J.E. Weiler, P.J. O'Brien, and D.H. MacLennan. 1991. Identification of a mutation in porcine ryanodine receptor associated with malignant hyperthermia. *Science*. 253:448–451. doi:10.1126/science.1862346

Furuichi, T., and K. Mikoshiba. 1995. Inositol 1, 4, 5-trisphosphate receptor-mediated Ca²⁺ signaling in the brain. *J. Neurochem.* 64:953–960. doi:10.1046/j.1471-4159.1995.64030953.x

Gao, L., D. Balshaw, L. Xu, A. Tripathy, C. Xin, and G. Meissner. 2000. Evidence for a role of the luminal M3–M4 loop in skeletal muscle Ca²⁺ release channel (ryanodine receptor) activity and conductance. *Biophys. J.* 79:828–840. doi:10.1016/S0006-3495(00)76339-9

Gillespie, D. 2008. Energetics of divalent selectivity in a calcium channel: the ryanodine receptor case study. *Biophys. J.* 94:1169–1184. doi:10.1529/biophysj.107.116798

Gillespie, D., and M. Fill. 2008. Intracellular calcium release channels mediate their own countercurrent: the ryanodine receptor case study. *Biophys. J.* 95:3706–3714. doi:10.1529/biophysj.108.131987

Gillespie, D., L. Xu, Y. Wang, and G. Meissner. 2005. (De)constructing the ryanodine receptor: modeling ion permeation and selectivity of the calcium release channel. *J. Phys. Chem. B*. 109:15598–15610. doi:10.1021/jp052471j

Goldberg, R.N., and R.L. Nuttall. 1978. Evaluated activity and osmotic coefficients for aqueous solutions: the alkaline earth metal halides. *J. Phys. Chem. Ref. Data*. 7:263–310. doi:10.1063/1.555569

Golding, E.M., and R.M. Golding. 1995. Interpretation of ³¹P MRS spectra in determining intracellular free magnesium and potassium ion concentrations. *Magn. Reson. Med.* 33:467–474. doi:10.1002/mrm.1910330403

Halvorson, H.R., A.M. Vande Linde, J.A. Helpern, and K.M. Welch. 1992. Assessment of magnesium concentrations by ³¹P NMR in vivo. *NMR Biomed.* 5:53–58. doi:10.1002/nbm.1940050202

Hamada, K., A. Terauchi, and K. Mikoshiba. 2003. Three-dimensional rearrangements within inositol 1,4,5-trisphosphate receptor by calcium. *J. Biol. Chem.* 278:52881–52889. doi:10.1074/jbc.M309743200

Hamer, W.J., and Y.-C. Wu. 1972. Osmotic coefficients and mean activity coefficients of uni-univalent electrolytes in water at 25°C. *J. Phys. Chem. Ref. Data*. 1:1047–1099. doi:10.1063/1.3253108

Hille, B. 2001. Ionic Channels of Excitable Membranes. 3rd edition. Sinauer Associates, Inc., Sunderland, MA. 814 pp.

Ionescu, L., K.H. Cheung, H. Vais, D.-O.D. Mak, C. White, and J.K. Foskett. 2006. Graded recruitment and inactivation of single InsP₃ receptor Ca²⁺-release channels: implications for quantal Ca²⁺ release. *J. Physiol.* 573:645–662. doi:10.1113/jphysiol.2006.109504

Iwasaki, H., K. Chiba, T. Uchiyama, F. Yoshikawa, F. Suzuki, M. Ikeda, T. Furuichi, and K. Mikoshiba. 2002. Molecular characterization of the starfish inositol 1,4,5-trisphosphate receptor and

its role during oocyte maturation and fertilization. *J. Biol. Chem.* 277:2763–2772. doi:10.1074/jbc.M108839200

Jiang, Q.X., E.C. Thrower, D.W. Chester, B.E. Ehrlich, and F.J. Sigworth. 2002. Three-dimensional structure of the type 1 inositol 1,4,5-trisphosphate receptor at 24 Å resolution. *EMBO J.* 21:3575–3581. doi:10.1093/emboj/cdf380

Joseph, S.K., and G. Hajnóczky. 2007. IP₃ receptors in cell survival and apoptosis: Ca²⁺ release and beyond. *Apoptosis.* 12:951–968. doi:10.1007/s10495-007-0719-7

Joseph, S.K., C. Lin, S. Pierson, A.P. Thomas, and A.R. Maranto. 1995. Heterooligomers of type-I and type-III inositol trisphosphate receptors in WB rat liver epithelial cells. *J. Biol. Chem.* 270:23310–23316. doi:10.1074/jbc.270.40.23310

Kaftan, E.J., B.E. Ehrlich, and J. Watras. 1997. Inositol 1,4,5-trisphosphate (InsP₃) and calcium interact to increase the dynamic range of InsP₃ receptor-dependent calcium signaling. *J. Gen. Physiol.* 110:529–538. doi:10.1085/jgp.110.5.529

Kettlun, C., A. González, E. Ríos, and M. Fill. 2003. Unitary Ca²⁺ current through mammalian cardiac and amphibian skeletal muscle ryanodine receptor channels under near-physiological ionic conditions. *J. Gen. Physiol.* 122:407–417. doi:10.1085/jgp.200308843

Lewis, C.A. 1979. Ion-concentration dependence of the reversal potential and the single channel conductance of ion channels at the frog neuromuscular junction. *J. Physiol.* 286:417–445.

Li, C., X. Wang, H. Vais, C.B. Thompson, J.K. Foskett, and C. White. 2007. Apoptosis regulation by Bcl-X_L modulation of mammalian inositol 1,4,5-trisphosphate receptor channel isoform gating. *Proc. Natl. Acad. Sci. USA.* 104:12565–12570. doi:10.1073/pnas.0702489104

Lindsay, A.R., S.D. Manning, and A.J. Williams. 1991. Monovalent cation conductance in the ryanodine receptor-channel of sheep cardiac muscle sarcoplasmic reticulum. *J. Physiol.* 439:463–480.

Mak, D.-O.D., and J.K. Foskett. 1994. Single-channel inositol 1,4,5-trisphosphate receptor currents revealed by patch clamp of isolated *Xenopus* oocyte nuclei. *J. Biol. Chem.* 269:29375–29378.

Mak, D.-O.D., and J.K. Foskett. 1997. Single-channel kinetics, inactivation, and spatial distribution of inositol trisphosphate (IP₃) receptors in *Xenopus* oocyte nucleus. *J. Gen. Physiol.* 109:571–587. doi:10.1085/jgp.109.5.571

Mak, D.-O.D., and J.K. Foskett. 1998. Effects of divalent cations on single-channel conduction properties of *Xenopus* IP₃ receptor. *Am. J. Physiol.* 275:C179–C188.

Mak, D.-O.D., S. McBride, and J.K. Foskett. 1998. Inositol 1,4,5-trisphosphate activation of inositol trisphosphate receptor Ca²⁺ channel by ligand tuning of Ca²⁺ inhibition. *Proc. Natl. Acad. Sci. USA.* 95:15821–15825. doi:10.1073/pnas.95.26.15821

Mak, D.-O.D., S. McBride, and J.K. Foskett. 1999. ATP regulation of type 1 inositol 1,4,5-trisphosphate receptor channel gating by allosteric tuning of Ca²⁺ activation. *J. Biol. Chem.* 274:22231–22237. doi:10.1074/jbc.274.32.22231

Mak, D.-O.D., S. McBride, V. Raghuram, Y. Yue, S.K. Joseph, and J.K. Foskett. 2000. Single-channel properties in endoplasmic reticulum membrane of recombinant type 3 inositol trisphosphate receptor. *J. Gen. Physiol.* 115:241–256. doi:10.1085/jgp.115.3.241

Mak, D.-O.D., S. McBride, and J.K. Foskett. 2001a. ATP regulation of recombinant type 3 inositol 1,4,5-trisphosphate receptor gating. *J. Gen. Physiol.* 117:447–456. doi:10.1085/jgp.117.5.447

Mak, D.-O.D., S. McBride, and J.K. Foskett. 2001b. Regulation by Ca²⁺ and inositol 1,4,5-trisphosphate (InsP₃) of single recombinant type 3 InsP₃ receptor channels. Ca²⁺ activation uniquely distinguishes types 1 and 3 InsP₃ receptors. *J. Gen. Physiol.* 117:435–446. doi:10.1085/jgp.117.5.435

Mak, D.-O.D., S.M. McBride, and J.K. Foskett. 2003. Spontaneous channel activity of the inositol 1,4,5-trisphosphate (InsP₃) receptor (InsP₃R). Application of allosteric modeling to calcium and InsP₃ regulation of InsP₃R single-channel gating. *J. Gen. Physiol.* 122:583–603. doi:10.1085/jgp.200308809

Mak, D.-O.D., C. White, L. Ionescu, and J.K. Foskett. 2005. Nuclear patch clamp electrophysiology of inositol trisphosphate receptor Ca²⁺ release channels. In *Calcium Signaling*. 2nd ed. J.W. Putney Jr., editor. CRC Press, Boca Raton, FL. 203–229.

Mak, D.-O.D., J.E. Pearson, K.P.C. Loong, S. Datta, M. Fernández-Mongil, and J.K. Foskett. 2007. Rapid ligand-regulated gating kinetics of single inositol 1,4,5-trisphosphate receptor Ca²⁺ release channels. *EMBO Rep.* 8:1044–1051. doi:10.1038/sj.embor.7401087

Marchenko, S.M., V.V. Yarotsky, T.N. Kovalenko, P.G. Kostyuk, and R.C. Thomas. 2005. Spontaneously active and InsP₃-activated ion channels in cell nuclei from rat cerebellar Purkinje and granule neurones. *J. Physiol.* 565:897–910. doi:10.1113/jphysiol.2004.081299

Marhl, M., S. Schuster, M. Brumen, and R. Heinrich. 1997. Modeling the interrelations between the calcium oscillations and ER membrane potential oscillations. *Biophys. Chem.* 63:221–239. doi:10.1016/S0301-4622(96)02248-X

Mignery, G.A., C.L. Newton, B.T. Archer III, and T.C. Südhof. 1990. Structure and expression of the rat inositol 1,4,5-trisphosphate receptor. *J. Biol. Chem.* 265:12679–12685.

Moraru, I.I., E.J. Kaftan, B.E. Ehrlich, and J. Watras. 1999. Regulation of type 1 inositol 1,4,5-trisphosphate-gated calcium channels by InsP₃ and calcium: simulation of single channel kinetics based on ligand binding and electrophysiological analysis. *J. Gen. Physiol.* 113:837–849. doi:10.1085/jgp.113.6.837

Morelle, B., J.M. Salmon, J. Vigo, and P. Viallet. 1994a. Are intracellular ionic concentrations accessible using fluorescent probes? The example of Mag-indo-1. *Cell Biol. Toxicol.* 10:339–344. doi:10.1007/BF00755780

Morelle, B., J.M. Salmon, J. Vigo, and P. Viallet. 1994b. Measurement of intracellular magnesium concentration in 3T3 fibroblasts with the fluorescent indicator Mag-indo-1. *Anal. Biochem.* 218:170–176. doi:10.1006/abio.1994.1156

Neher, E. 1995. Voltage offsets in patch-clamp experiments. In *Single-channel recording*. 2nd edition. B. Sakmann and E. Neher, editors. Plenum Press, New York. 147–153.

Neher, E. 1998. Usefulness and limitations of linear approximations to the understanding of Ca²⁺ signals. *Cell Calcium.* 24:345–357. doi:10.1016/S0143-4160(98)90058-6

Palmer, A.E., C. Jin, J.C. Reed, and R.Y. Tsien. 2004. Bcl-2-mediated alterations in endoplasmic reticulum Ca²⁺ analyzed with an improved genetically encoded fluorescent sensor. *Proc. Natl. Acad. Sci. USA.* 101:17404–17409. doi:10.1073/pnas.0408030101

Patterson, R.L., D. Boehning, and S.H. Snyder. 2004. Inositol 1,4,5-trisphosphate receptors as signal integrators. *Annu. Rev. Biochem.* 73:437–465. doi:10.1146/annurev.biochem.73.071403.161303

Rahman, T., and C.W. Taylor. 2009. Dynamic regulation of IP₃ receptor clustering and activity by IP₃. *Channels (Austin).* 3:226–232.

Randriamampita, C., and A. Trautmann. 2004. Ca²⁺ signals and T lymphocytes; “New mechanisms and functions in Ca²⁺ signalling”. *Biol. Cell.* 96:69–78. doi:10.1016/j.biolcel.2003.10.008

Sato, C., K. Hamada, T. Ogura, A. Miyazawa, K. Iwasaki, Y. Hiroaki, K. Tani, A. Terauchi, Y. Fujiyoshi, and K. Mikoshiba. 2004. Inositol 1,4,5-trisphosphate receptor contains multiple cavities and L-shaped ligand-binding domains. *J. Mol. Biol.* 336:155–164. doi:10.1016/j.jmb.2003.11.024

Serysheva, I.I., D.J. Bare, S.J. Ludtke, C.S. Kettlun, W. Chiu, and G.A. Mignery. 2003. Structure of the type 1 inositol 1,4,5-trisphosphate receptor revealed by electron cryomicroscopy. *J. Biol. Chem.* 278:21319–21322. doi:10.1074/jbc.C300148200

Shuai, J., H.J. Rose, and I. Parker. 2006. The number and spatial distribution of IP₃ receptors underlying calcium puffs in *Xenopus* oocytes. *Biophys. J.* 91:4033–4044. doi:10.1529/biophysj.106.088880

Shuai, J., J.E. Pearson, and I. Parker. 2008. Modeling Ca^{2+} feedback on a single inositol 1,4,5-trisphosphate receptor and its modulation by Ca^{2+} buffers. *Biophys. J.* 95:3738–3752. doi:10.1529/biophysj.108.137182

Silverman, H.S., F. Di Lisa, R.C. Hui, H. Miyata, S.J. Sollott, R.G. Hanford, E.G. Lakatta, and M.D. Stern. 1994. Regulation of intracellular free Mg^{2+} and contraction in single adult mammalian cardiac myocytes. *Am. J. Physiol.* 266:C222–C233.

Singh, J., and D.M. Wisdom. 1995. Second messenger role of magnesium in pancreatic acinar cells of the rat. *Mol. Cell. Biochem.* 149:175–182. doi:10.1007/BF01076575

Smith, G.D. 1996. Analytical steady-state solution to the rapid buffering approximation near an open Ca^{2+} channel. *Biophys. J.* 71:3064–3072. doi:10.1016/S0006-3495(96)79500-0

Smith, G.D., J. Wagner, and J. Keizer. 1996. Validity of the rapid buffering approximation near a point source of calcium ions. *Biophys. J.* 70:2527–2539. doi:10.1016/S0006-3495(96)79824-7

Smith, I.F., and I. Parker. 2009. Imaging the quantal substructure of single IP_3R channel activity during Ca^{2+} puffs in intact mammalian cells. *Proc. Natl. Acad. Sci. USA.* 106:6404–6409. doi:10.1073/pnas.0810799106

Sneyd, J., and M. Falcke. 2005. Models of the inositol trisphosphate receptor. *Prog. Biophys. Mol. Biol.* 89:207–245. doi:10.1016/j.pbiomolbio.2004.11.001

Sugawara, H., M. Kurosaki, M. Takata, and T. Kurosaki. 1997. Genetic evidence for involvement of type 1, type 2 and type 3 inositol 1,4,5-trisphosphate receptors in signal transduction through the B-cell antigen receptor. *EMBO J.* 16:3078–3088. doi:10.1093/emboj/16.11.3078

Sun, X.P., N. Callamaras, J.S. Marchant, and I. Parker. 1998. A continuum of InsP_3 -mediated elementary Ca^{2+} signalling events in *Xenopus* oocytes. *J. Physiol.* 509:67–80. doi:10.1111/j.1469-7793.1998.067bo.x

Swaminathan, D., G. Ullah, and P. Jung. 2009. A simple sequential-binding model for calcium puffs. *Chaos.* 19:037109. doi:10.1063/1.3152227

Swillens, S., L. Combettes, and P. Champeil. 1994. Transient inositol 1,4,5-trisphosphate-induced Ca^{2+} release: a model based on regulatory Ca^{2+} -binding sites along the permeation pathway. *Proc. Natl. Acad. Sci. USA.* 91:10074–10078. doi:10.1073/pnas.91.21.10074

Swillens, S., P. Champeil, L. Combettes, and G. Dupont. 1998. Stochastic simulation of a single inositol 1,4,5-trisphosphate-sensitive Ca^{2+} channel reveals repetitive openings during ‘blip-like’ Ca^{2+} transients. *Cell Calcium.* 23:291–302. doi:10.1016/S0143-4160(98)90025-2

Swillens, S., G. Dupont, L. Combettes, and P. Champeil. 1999. From calcium blips to calcium puffs: theoretical analysis of the requirements for interchannel communication. *Proc. Natl. Acad. Sci. USA.* 96:13750–13755. doi:10.1073/pnas.96.24.13750

Tang, Y., J.L. Stephenson, and H.G. Othmer. 1996. Simplification and analysis of models of calcium dynamics based on IP_3 -sensitive calcium channel kinetics. *Biophys. J.* 70:246–263. doi:10.1016/S0006-3495(96)79567-X

Tashiro, M., and M. Konishi. 1997. Basal intracellular free Mg^{2+} concentration in smooth muscle cells of guinea pig tenia cecum: intracellular calibration of the fluorescent indicator furaptra. *Biophys. J.* 73:3358–3370. doi:10.1016/S0006-3495(97)78360-7

Taufiq-Ur-Rahman, A. Skupin, M. Falcke, and C.W. Taylor. 2009. Clustering of InsP_3 receptors by InsP_3 retunes their regulation by InsP_3 and Ca^{2+} . *Nature.* 458:655–659. doi:10.1038/nature07763

Taylor, C.W., and A. Richardson. 1991. Structure and function of inositol trisphosphate receptors. *Pharmacol. Ther.* 51:97–137. doi:10.1016/0163-7258(91)90043-L

Thul, R., and M. Falcke. 2004. Release currents of IP_3 receptor channel clusters and concentration profiles. *Biophys. J.* 86:2660–2673. doi:10.1016/S0006-3495(04)74322-2

Tinker, A., A.R. Lindsay, and A.J. Williams. 1992. A model for ionic conduction in the ryanodine receptor channel of sheep cardiac muscle sarcoplasmic reticulum. *J. Gen. Physiol.* 100:495–517. doi:10.1085/jgp.100.3.495

Vais, H., A.P. Siebert, Z. Ma, M. Fernández-Mongil, J.K. Foskett, and D.-O.D. Mak. 2010. Redox-regulated heterogeneous thresholds for ligand recruitment among InsP_3R Ca^{2+} -release channels. *Biophys. J.* 99:407–416. doi:10.1016/j.bpj.2010.04.034

Wagner, J., and J. Keizer. 1994. Effects of rapid buffers on Ca^{2+} diffusion and Ca^{2+} oscillations. *Biophys. J.* 67:447–456. doi:10.1016/S0006-3495(94)80500-4

Wang, Y., L. Xu, D.A. Pasek, D. Gillespie, and G. Meissner. 2005. Probing the role of negatively charged amino acid residues in ion permeation of skeletal muscle ryanodine receptor. *Biophys. J.* 89:256–265. doi:10.1529/biophysj.104.056002

Watras, J., I. Bezprozvanny, and B.E. Ehrlich. 1991. Inositol 1,4,5-trisphosphate-gated channels in cerebellum: presence of multiple conductance states. *J. Neurosci.* 11:3239–3245.

Wolfram, F., E. Morris, and C.W. Taylor. 2010. Three-dimensional structure of recombinant type 1 inositol 1,4,5-trisphosphate receptor. *Biochem. J.* 428:483–489. doi:10.1042/BJ20100143

Xu, L., Y. Wang, D. Gillespie, and G. Meissner. 2006. Two rings of negative charges in the cytosolic vestibule of type-1 ryanodine receptor modulate ion fluxes. *Biophys. J.* 90:443–453. doi:10.1529/biophysj.105.072538

Yoshikawa, S., T. Tanimura, A. Miyawaki, M. Nakamura, M. Yuzaki, T. Furuchi, and K. Mikoshiba. 1992. Molecular cloning and characterization of the inositol 1,4,5-trisphosphate receptor in *Drosophila melanogaster*. *J. Biol. Chem.* 267:16613–16619.

Yu, R., and P.M. Hinkle. 2000. Rapid turnover of calcium in the endoplasmic reticulum during signaling. Studies with cameleon calcium indicators. *J. Biol. Chem.* 275:23648–23653. doi:10.1074/jbc.M002684200

Zhao, M., P. Li, X. Li, L. Zhang, R.J. Winkfein, and S.R. Chen. 1999. Molecular identification of the ryanodine receptor pore-forming segment. *J. Biol. Chem.* 274:25971–25974. doi:10.1074/jbc.274.37.25971

Zorzato, F., J. Fujii, K. Otsu, M. Phillips, N.M. Green, F.A. Lai, G. Meissner, and D.H. MacLennan. 1990. Molecular cloning of cDNA encoding human and rabbit forms of the Ca^{2+} release channel (ryanodine receptor) of skeletal muscle sarcoplasmic reticulum. *J. Biol. Chem.* 265:2244–2256.